Beam-forming choices: what are they, how do they work, and what is their impact for elastography

Marvin M. Doyley
University of Rochester
Hajim School of Engineering & Applied Sciences
Department of Electrical & Computer Engineering

Elastography

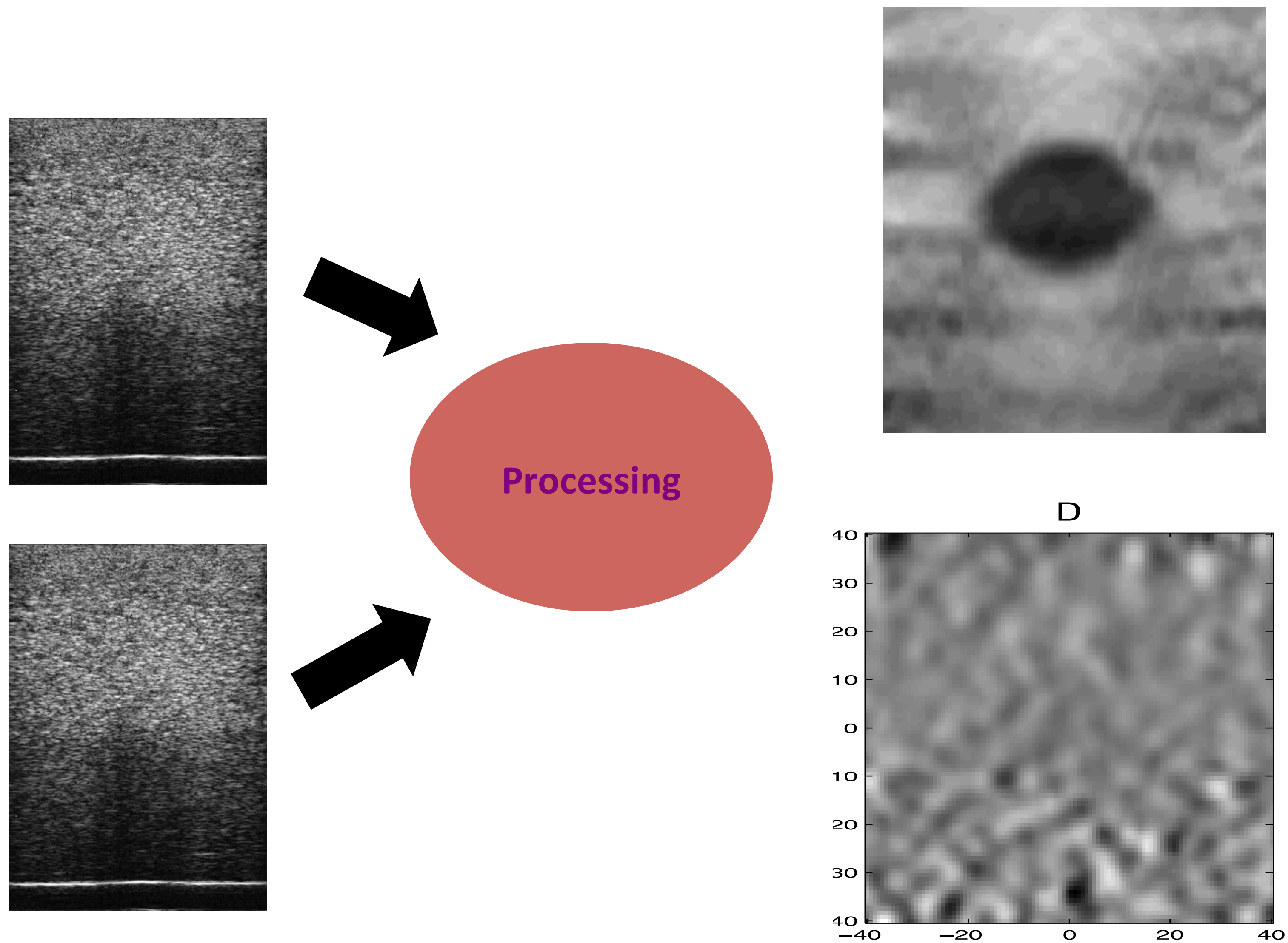

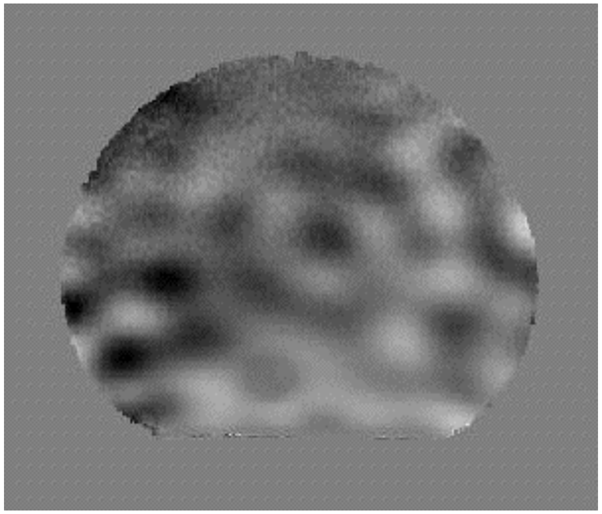

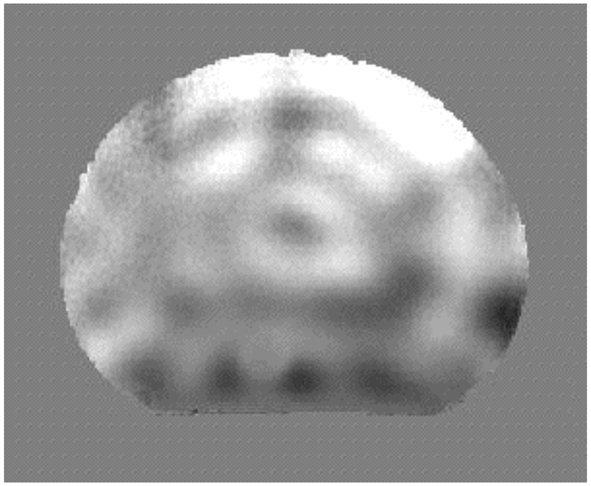

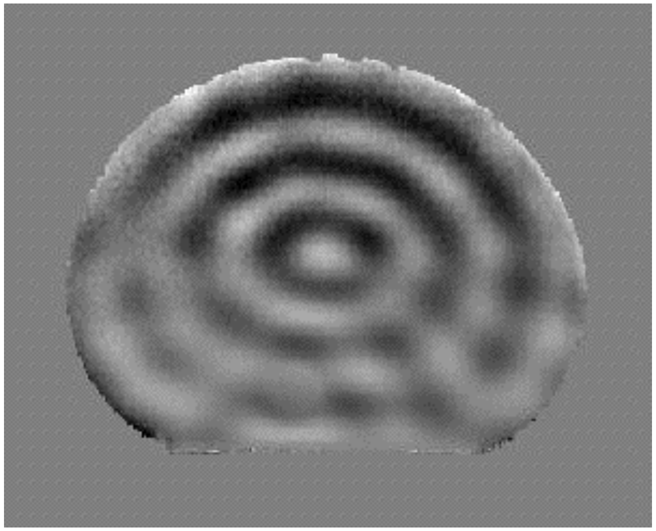

PSF- Achilles's heel

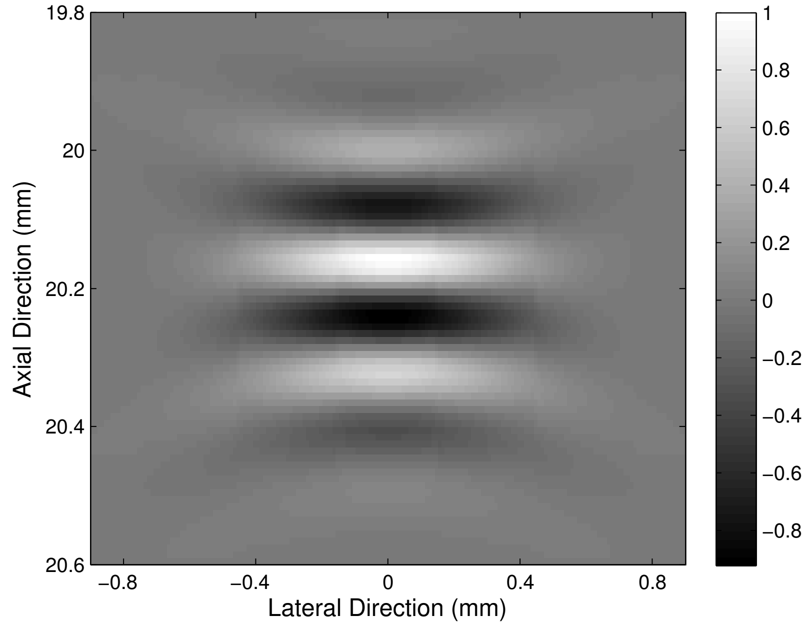

$$\hat{f}(x,y) = \int_{-\infty}^{\infty}\int_{-\infty}^{\infty} f(\alpha,\beta)h(x-\alpha,y-\beta)\,d\alpha\, d\beta + \eta(x,y)$$

$$\hat{f}(x,y) = h(x,y) \otimes f(x,y) + \eta(x,y)$$

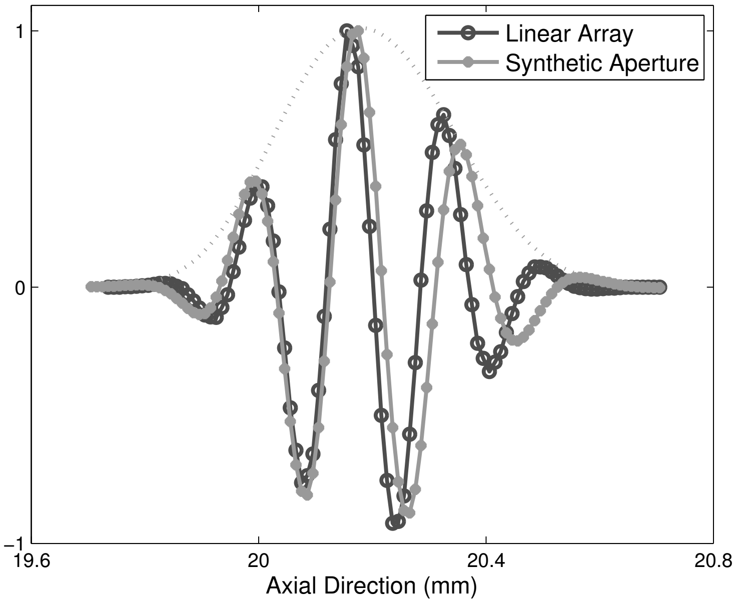

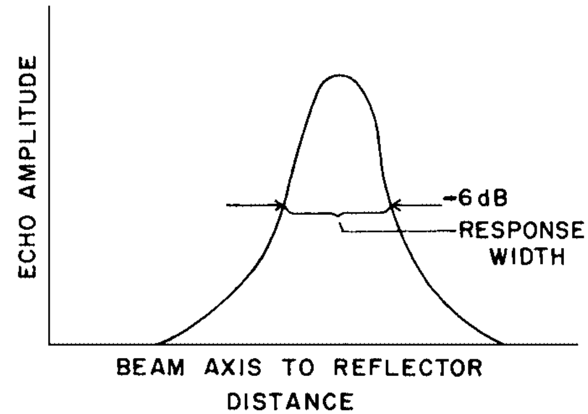

(a)

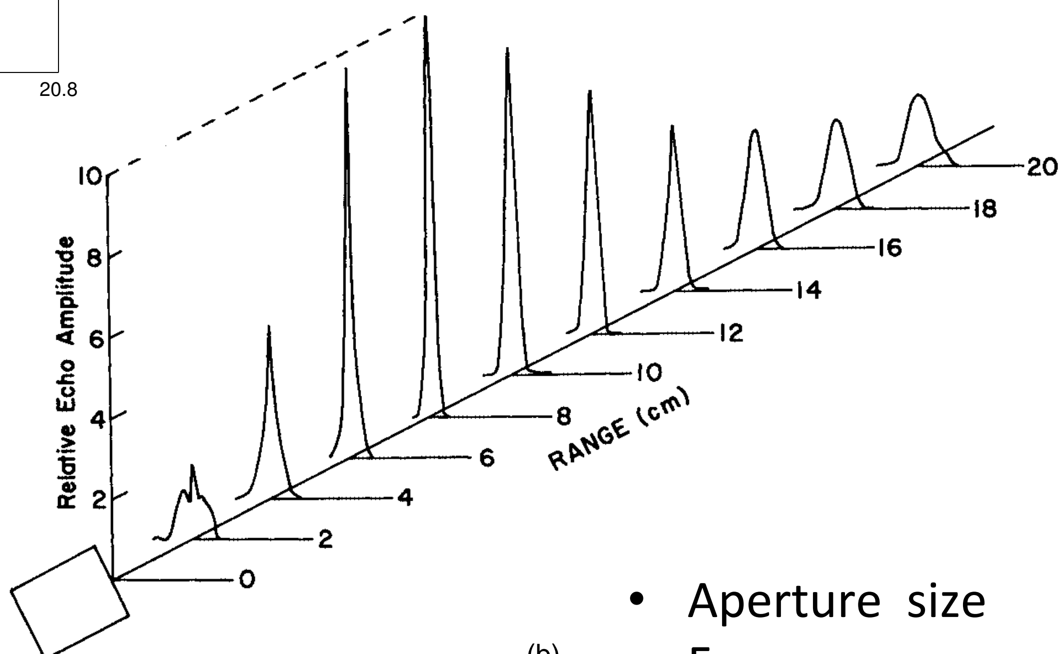

(b)

- Aperture size
- Focus
- Scan depth

Correspondence

A Deconvolution Filter for Improvement of Time-Delay Estimation in Elastography

S. Kaisar Alam, *Senior Member, IEEE*, Jonathan Ophir, *Member, IEEE*, Ignacio Céspedes, *Member, IEEE*, and Tomy Varghese, *Member, IEEE*

***Abstract*—In elastography, tissue under investigation is compressed, and the resulting strain is estimated from the gradient of displacement estimates. Therefore, it is important to accurately estimate the displacements (time-delay) for good quality elastograms. A principal source of error in time-delay estimation in elastography is the decorrelation of the echo signal due to tissue compression (decorrelation noise). Temporal stretching of the postcompression signals has been shown to reduce the decorrelation noise at small strains. In this article, we present a deconvolution filter that reduces the decorrelation even further when applied in conjunction with signal stretching. The performance of the proposed filter is evaluated using simulated data.**

I. Introduction

reduce decorrelation due to nonaxial tissue motion, and thus reduce the dimensionality of the problem. The errors due to PSF deformation become significant when the dimensionality of the problem is reduced. In this article, we demonstrate the correlation enhancement obtained by processing the postcompression signal with a deconvolution filter following the temporal stretching step.

We propose an inverse filter approach for the deconvolution. It can be shown that the inverse filter is a special case of the optimal Wiener filter that can be used in deconvolution problems. The Wiener filter can be expressed as follows [12]:

$$H_{\text{Wiener}}(f) = \frac{P^*(f)}{|P(f)|^2 + \frac{S_n(f)}{S_r(f)}}$$

where $P(f)$ is the transfer function of the system, $S_n(f)$ is the noise power spectral density, and $S_r(f)$ is the power spectral density of the random distribution that the scatterers are part of. Depending on the signal-to-noise ratio (SNR), there can be two extreme cases of this Wiener filter [13]. When the SNR is very high, $S_n(f)/S_r(f)$ can be neglected, and $P^*(f)$ cancels from the numerator and denominator, resulting in the classical inverse filter we have used in this paper:

Very Hard problem to solve !

Ultrasound in Med. & Biol., Vol. 24, No. 8, pp. 1183–1199, 1998

0301-5629/98 $19.00 + .00

ELSEVIER

PII S0301-5629(98)00109-4

● *Original Contribution*

A NEW ELASTOGRAPHIC METHOD FOR ESTIMATION AND IMAGING OF LATERAL DISPLACEMENTS, LATERAL STRAINS, CORRECTED AXIAL STRAINS AND POISSON'S RATIOS IN TISSUES

ELISA KONOFAGOU*‡ and JONATHAN OPHIR*†‡

*Ultrasonics Laboratory, Department of Radiology, The University of Texas Medical School, Houston, TX 77030 USA; and †Department of Electrical Engineering and ‡Program in Biomedical Engineering, University of Houston, Houston, TX 77204 USA

(*Received* 31 *December* 1997; *in final form* 15 *June* 1998)

Abstract—A major disadvantage of the current practice of elastography is that only the axial component of the strain is estimated. The lateral and elevational components are basically disregarded, yet they corrupt the axial strain estimation by inducing decorrelation noise. In this paper, we describe a new weighted interpolation method operating between neighboring RF A-lines for high precision tracking of the lateral displacement. Due to this high lateral-tracking precision, quality lateral elastograms are generated that display the lateral component of the strain tensor. These precision lateral-displacement estimates allow a fine correction for the lateral decorrelation that corrupts the axial estimation. Finally, by dividing the lateral elastogram by the axial elastogram, we are able to produce a new image that displays the distribution of Poisson's ratios in the tissue. Results are presented from finite-element simulations and phantoms as well as in vitro and in vivo experiments. © 1998 World Federation for Ultrasound in Medicine & Biology.

Key Words: **Correction, Displacement, Elasticity, Elastic modulus, Elastogram, Elastography, Imaging, Interpolation, Lateral, Poisson's ratio, Shear, Strain, Tracking, Ultrasound.**

Beam Steering

IEEE TRANSACTIONS ON MEDICAL IMAGING, VOL. 23, NO. 12, DECEMBER 2004 1479

Estimation of Displacement Vectors and Strain Tensors in Elastography Using Angular Insonifications

U. Techavipoo, Q. Chen, T. Varghese*, and J. A. Zagzebski

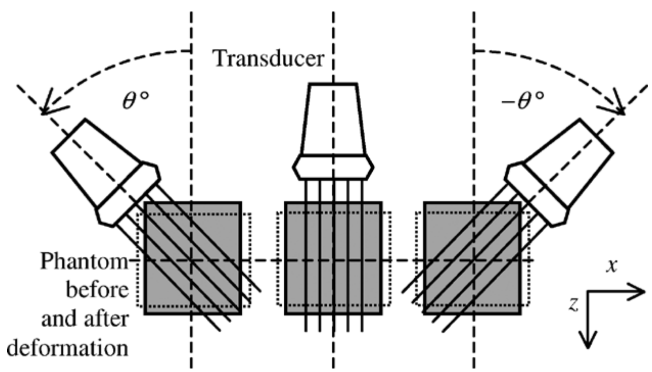

Fig. 4. Simulation model for strain tensor estimation. A linear transducer rotates for every 1° around the center of the phantom, from −45° to 45°. RF signals are generated for each location of the transducer before and after phantom deformation.

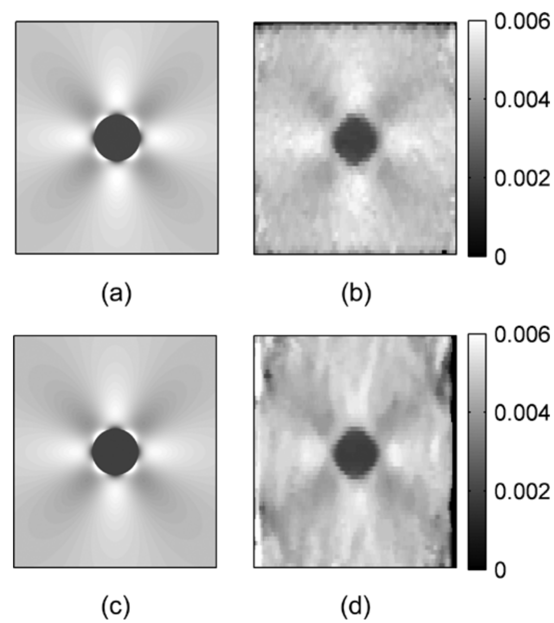

Fig. 9. Ideal and estimated axial strain images in (a) and (b), respectively, and ideal and estimated lateral strain images in (c) and (d), respectively.

Noninvasive Carotid Strain Imaging Using Angular Compounding at Large Beam Steered Angles: Validation in Vessel Phantoms

Hendrik H. G. Hansen*, Richard G. P. Lopata, and Chris L. de Korte

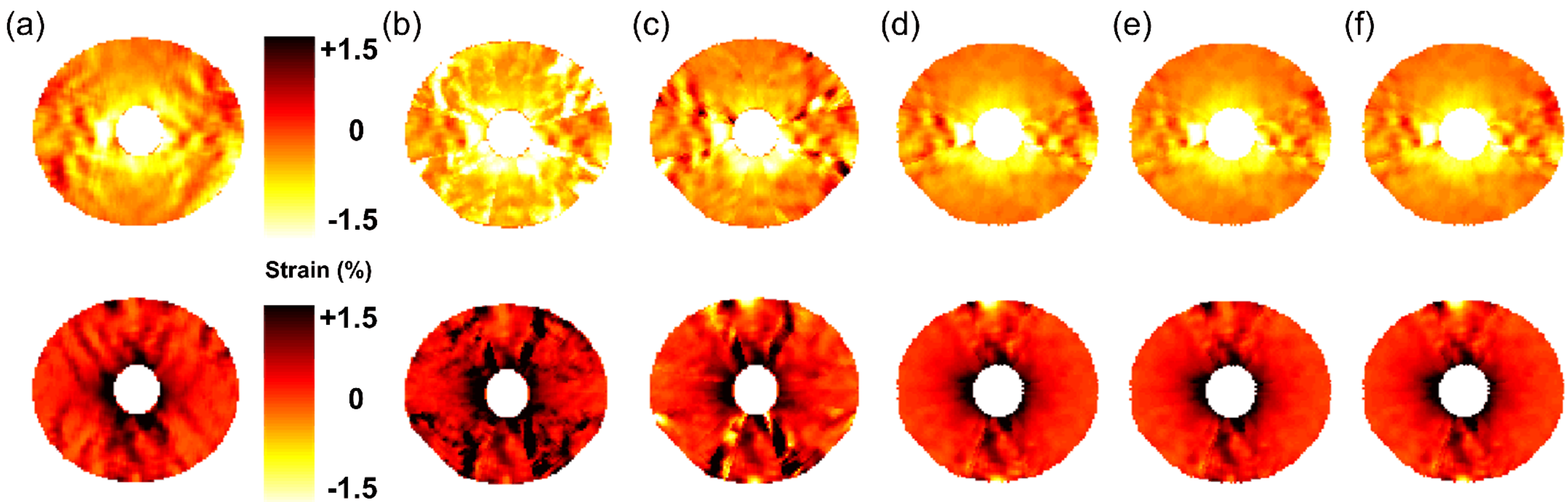

Fig. 5. Radial (top row) and circumferential (bottom row) strain images for a concentric homogeneous vessel phantom. (a) Radial and circumferential strain images calculated by principal component analysis from 0° data only. (b)–(f) Compound radial and circumferential strain images constructed by principal component analysis, application of the rotation matrices, projection of axial and lateral strain, projection of axial strain completed with a segment of principal component analysis, projection of axial strain completed with a segment obtained from the rotation matrices.

Can we change the PSF ?

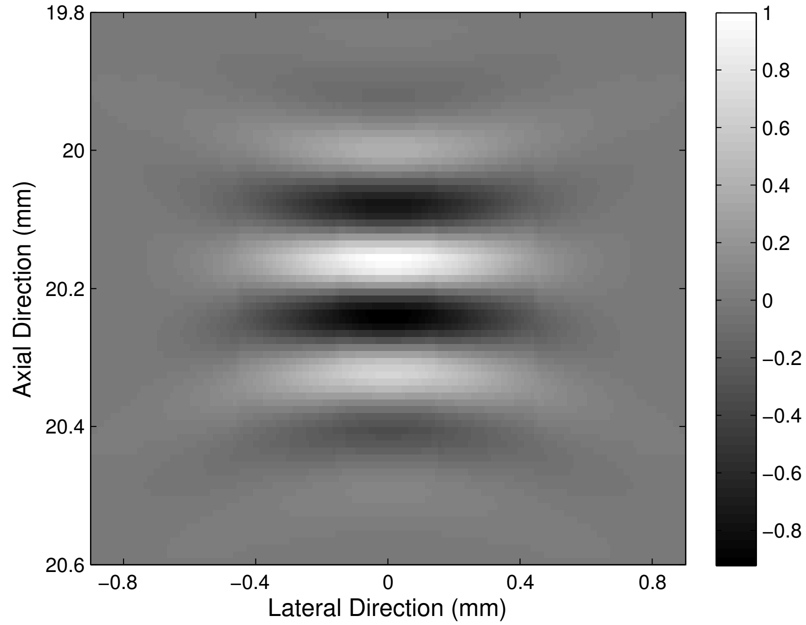

$$\hat{f}(x,y) = \int_{-\infty}^{\infty}\int_{-\infty}^{\infty} f(\alpha,\beta)h(x-\alpha,y-\beta)\,d\alpha\, d\beta + \eta(x,y)$$

$$\hat{f}(x,y) = h(x,y) \otimes f(x,y) + \eta(x,y)$$

Beam-forming + Research scanners

- Introduce oscillation in lateral or elevation direction
- Reduce the lateral and elevation extent of the PS

Beamforming Basics

Each element samples the propagating wave spatially. Therefore, the goal of the beam-forming is to detect a signal in the presence of noise and Interfering signal.

Beamformer perform spatial filtering to separate signals that have overlapping frequency content that original from different spatial location.

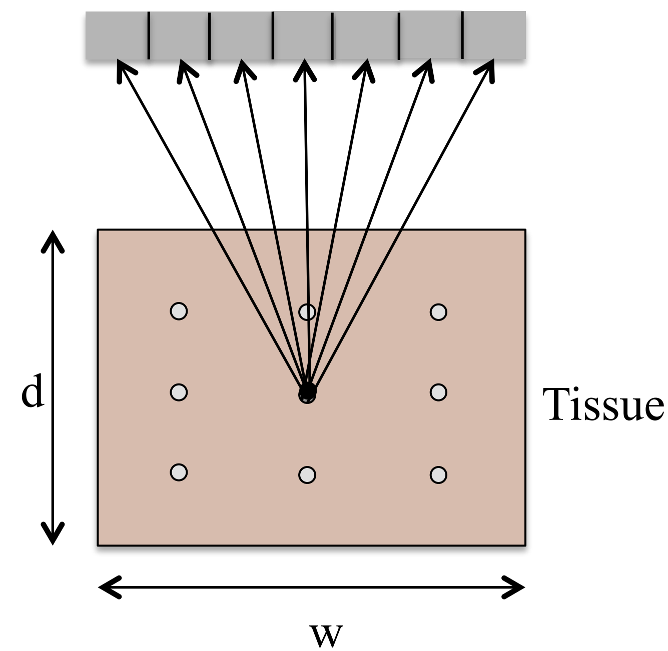

Applications

1. Communication systems
2. Hearing aid design
3. Oil exploration
4. Sonar and Radar

Thomenius 1996 IEEE UFFC Evolution of ultrasound beamformers
Van Veen and Buckley IEEE ASSP 1988

Delay-and-sum beam-former

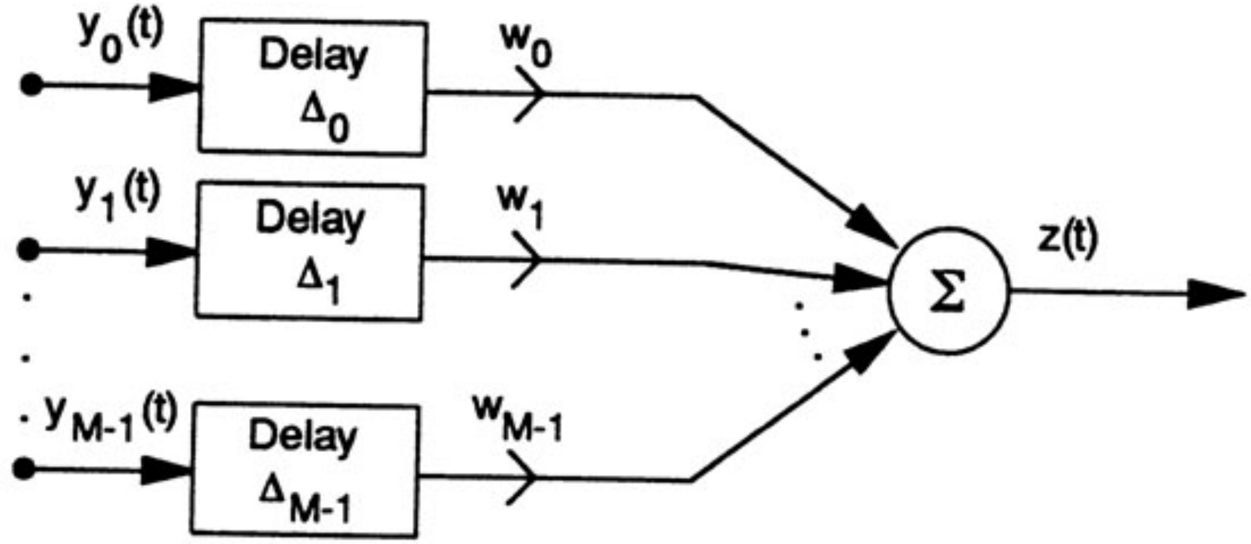

$$z(t) = \sum_{m=0}^{M-1} w_m y_m (t - \Delta_m)$$

Apodization

Delay

Real-system

$$s(\mathbf{P}) = \sum_{i=1}^{N_{tx}} \sum_{j=1}^{N_{rx}} w_{tx}(i) w_{rx}(j) T_{ij}(t - \tau_P)$$

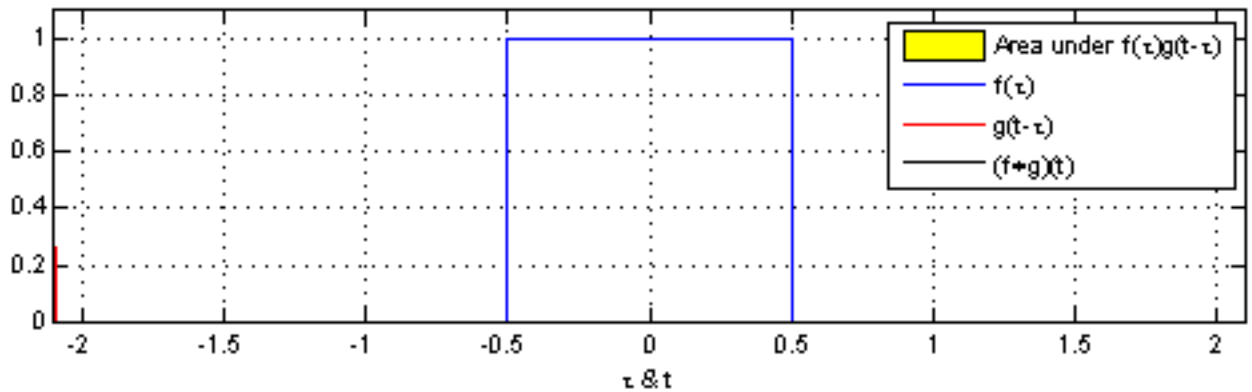

Effective Aperture

Delay calculation (fix focus)

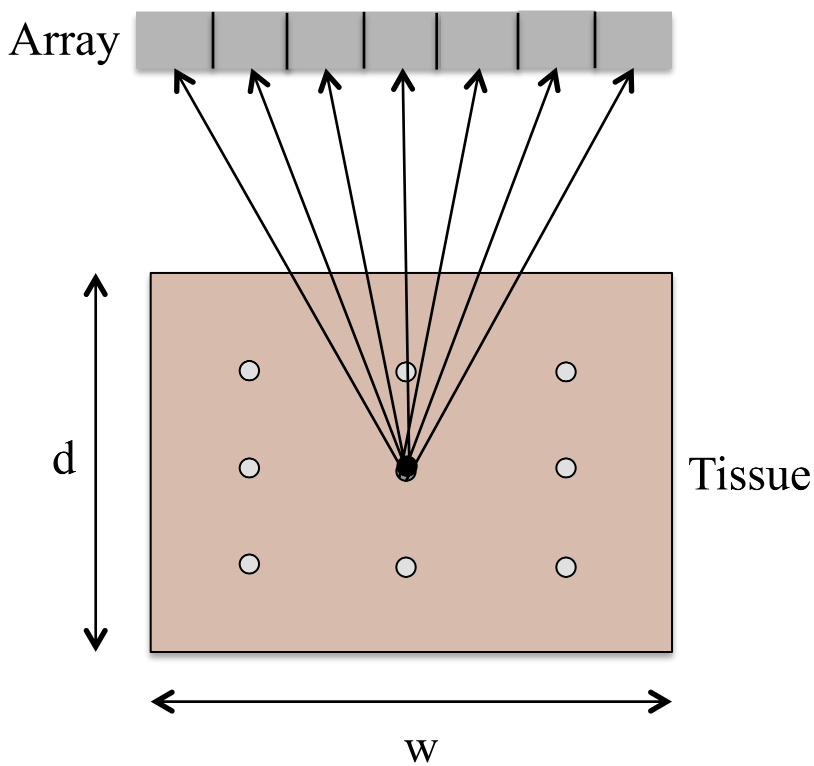

Path difference: simple geometric calculations

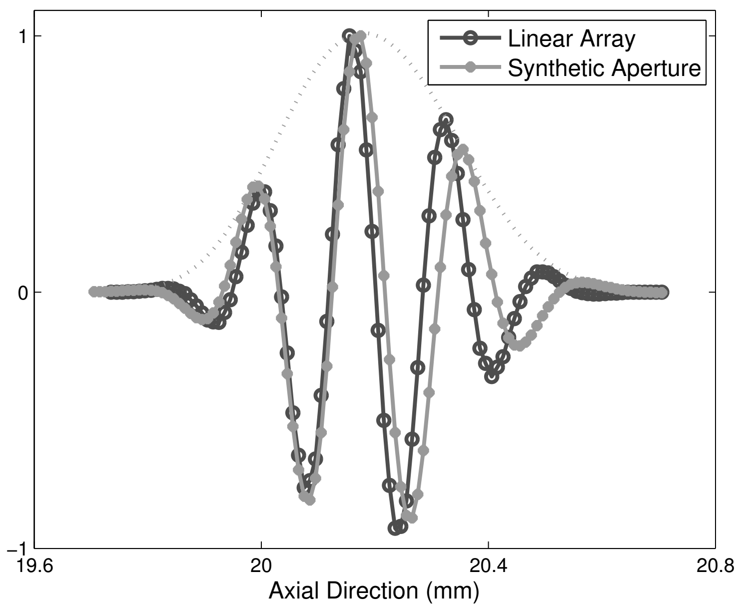

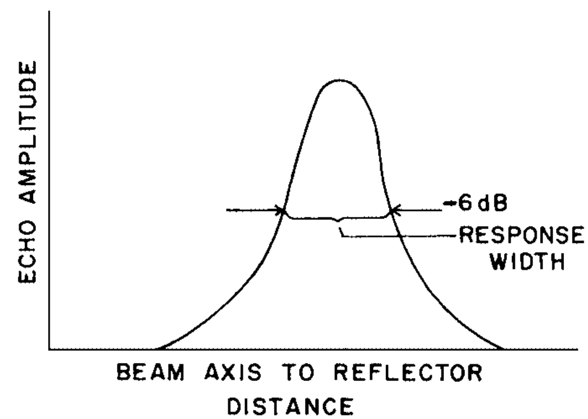

(a)

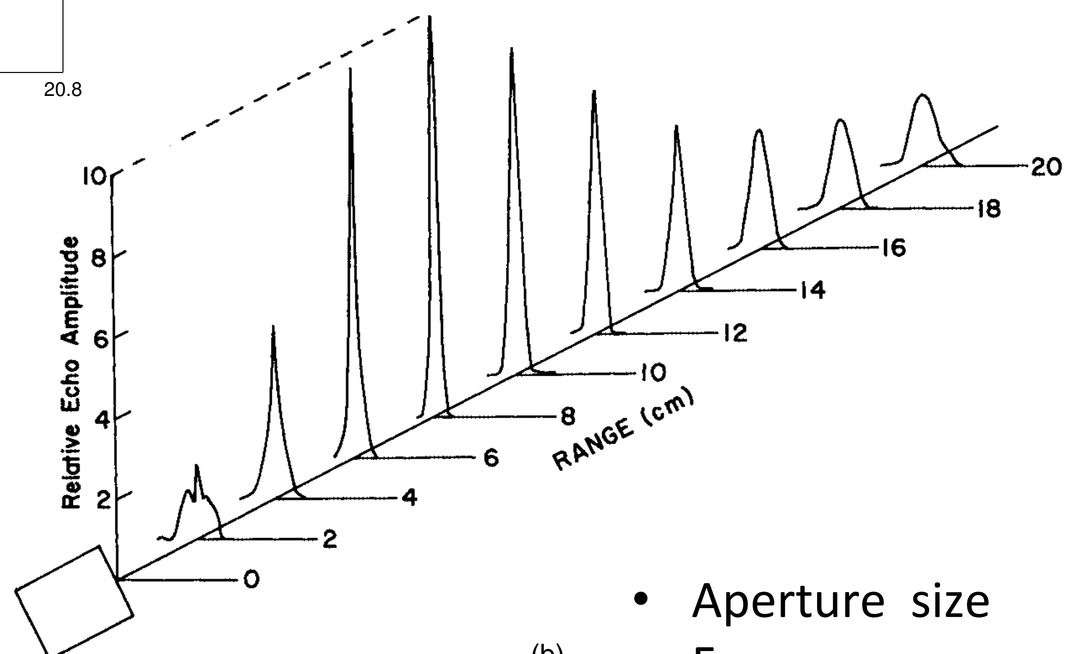

(b)

- Aperture size
- Focus
- Scan depth

Dynamic focusing (calculate delay for every point)

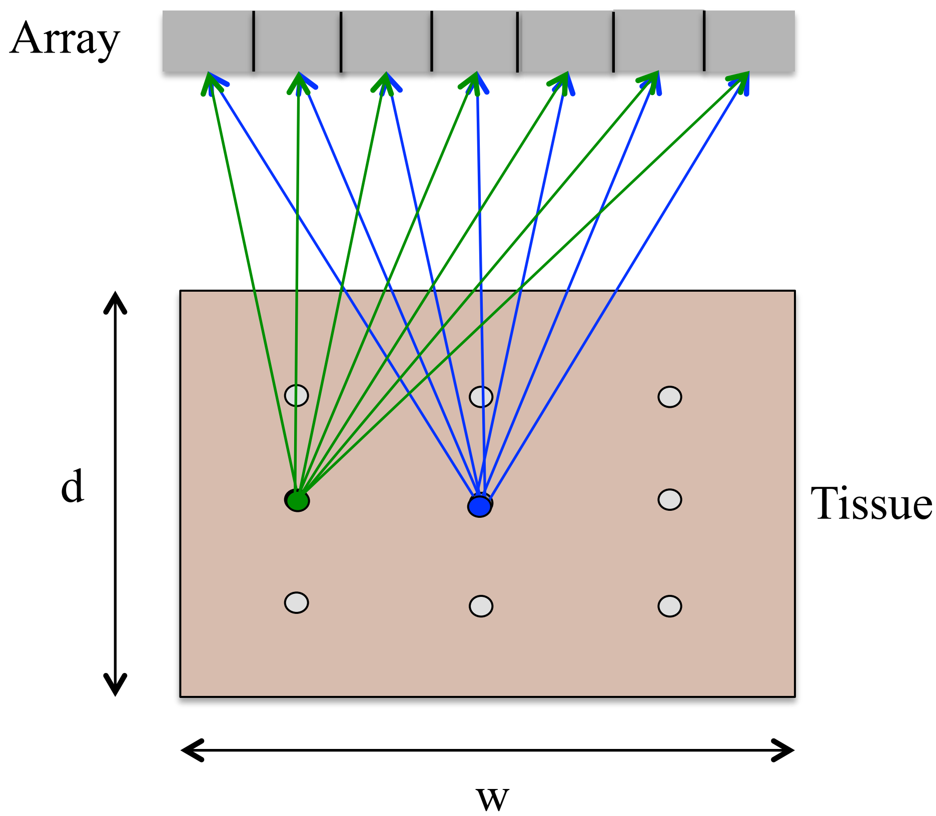

To separate signal with overlapping freq. comp

Actual response

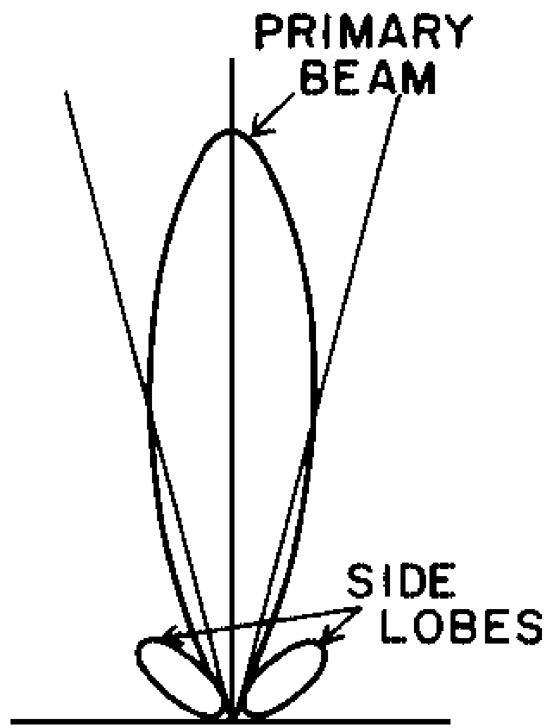

Minimize the squared difference between the actual and desired freq. response

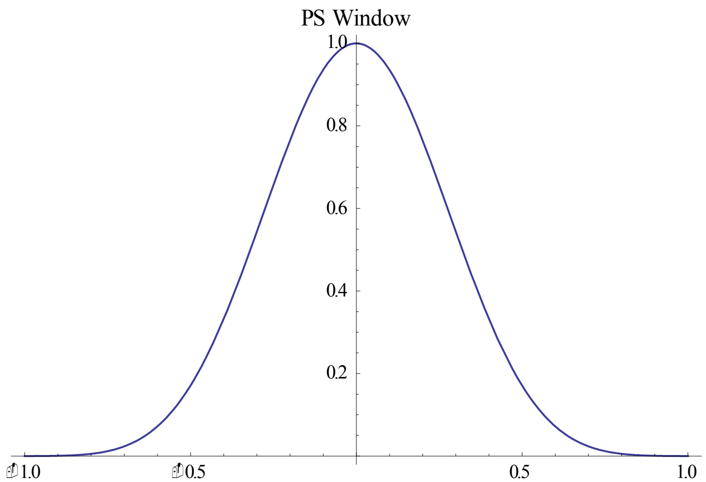
PS Window
1.0
0.8
0.6
0.4
0.2
-1.0
-0.5
0.5
1.0

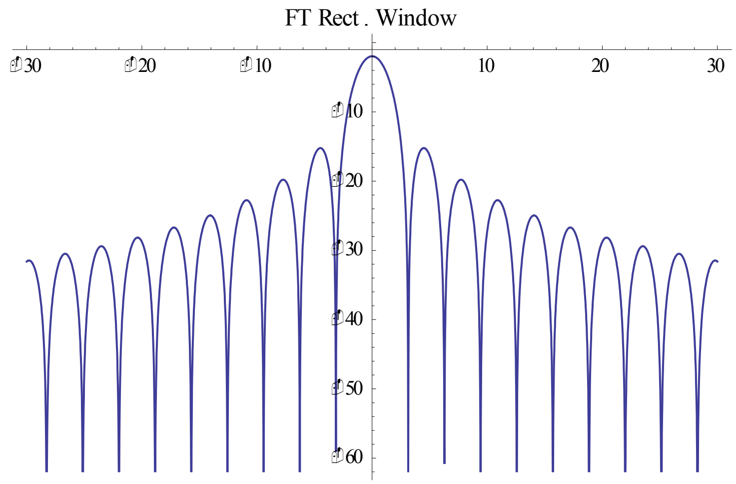
FT Rect. Window
-30
-20
-10
10
20
30
-10
-20
-30
-40
-50
-60

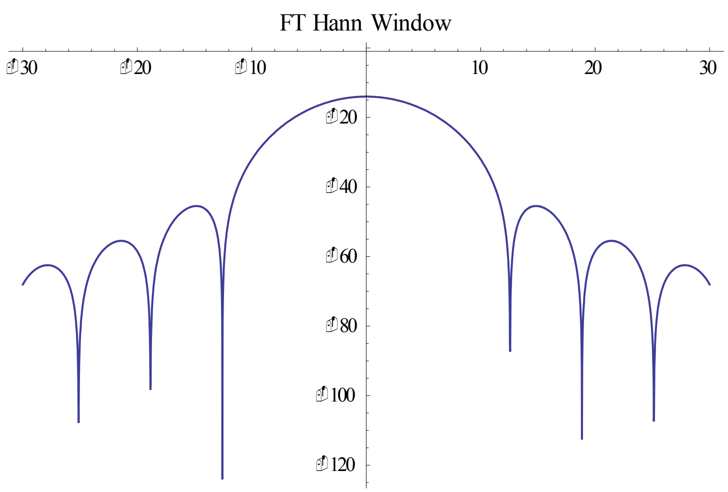
FT Hann Window
-30
-20
-10
10
20
30
-20
-40
-60
-80
-100
-120

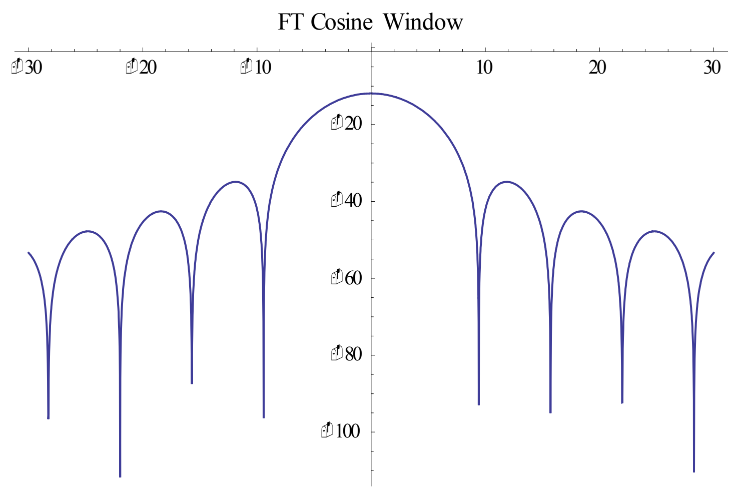
FT Cosine Window
-30
-20
-10
10
20
30
-20
-40
-60
-80
-100

Performance of different apodization functions

TABLE I. EVALUATION OF SELECTED APODIZATION FUNCTIONS.

	Criteria 1 Limited support	Criteria 2 Energy (% of maximum)	Criteria 3 −6-dB beamwidth (normalized units)	Criteria 3 Side lobe maximum level (dB)
Rect	Yes	100	3.8	−13
Gauss 5σ	By truncation	70	6.0	−43
Blackman	Yes	60	7.2	−57
Sinh^5	Yes	48	8.6	−78

Field II simulation 5 MHz (f # 3.2) point scatters at focus, 60 mm depth

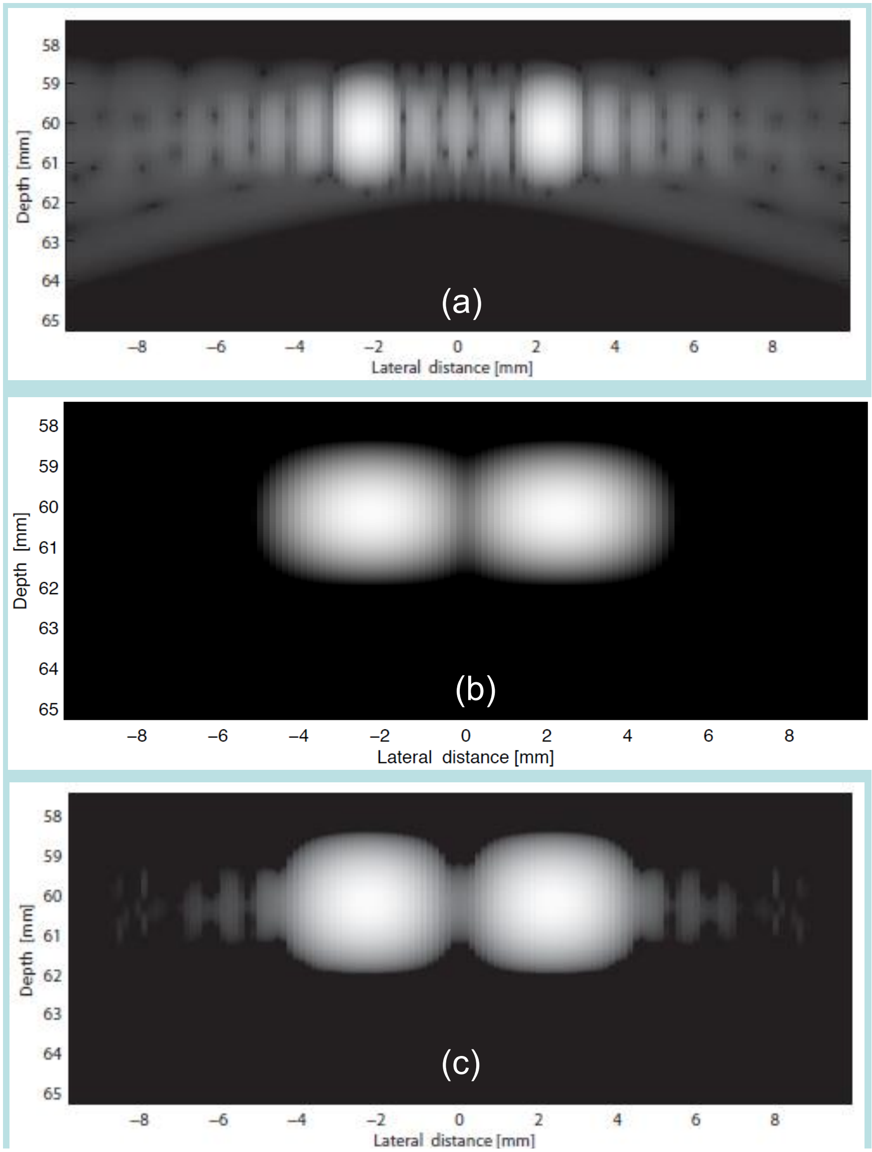

Box-car

$\sinh^5$

Truncated Gaussian

Prolate Spherodial function

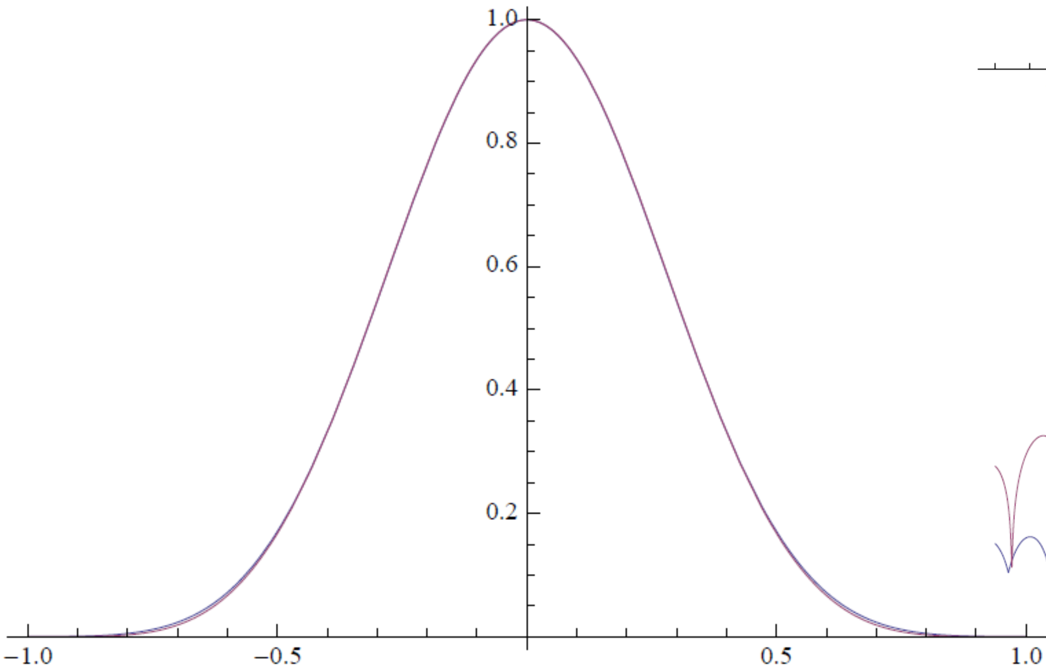

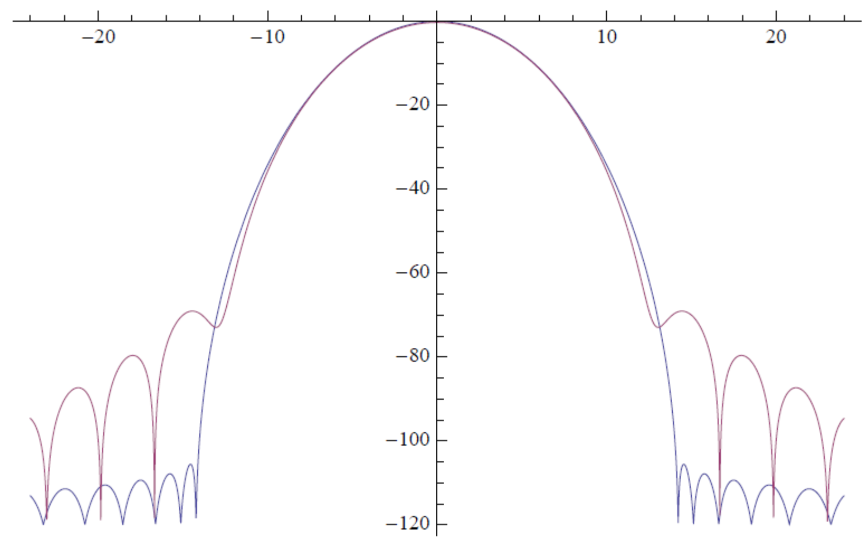

$$\int_{-t_o}^{t_o} \psi_n(c,t)\frac{\sin\Omega(x-t)}{\pi(x-t)}dt = \psi_n(c,x)\lambda_n(c)$$

In time domain very little difference to side-lobe PSW – 110 dB

Synthetic Aperture Imaging

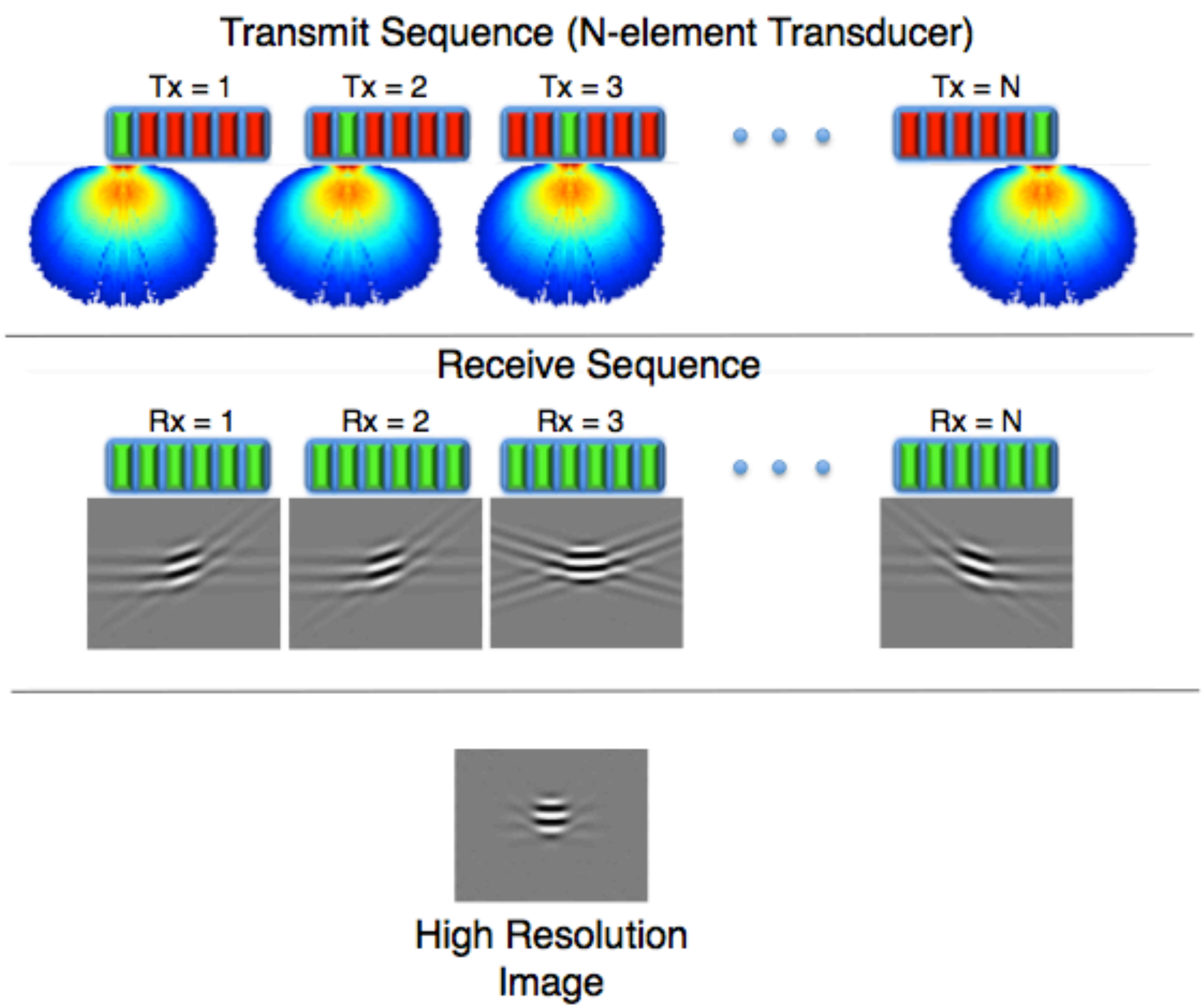

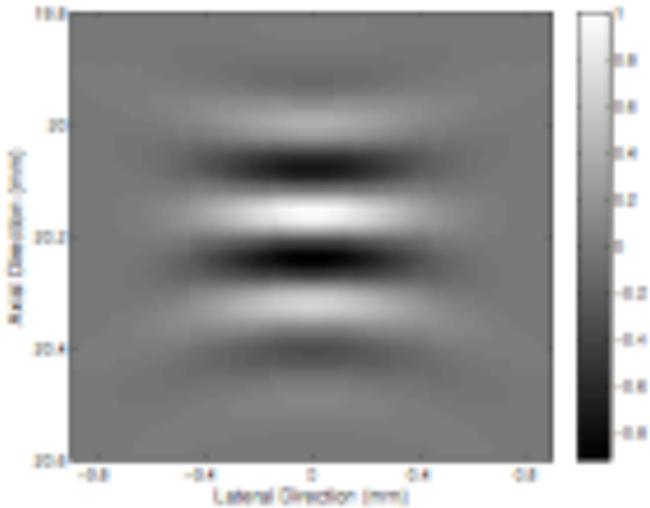

(a) Linear Array

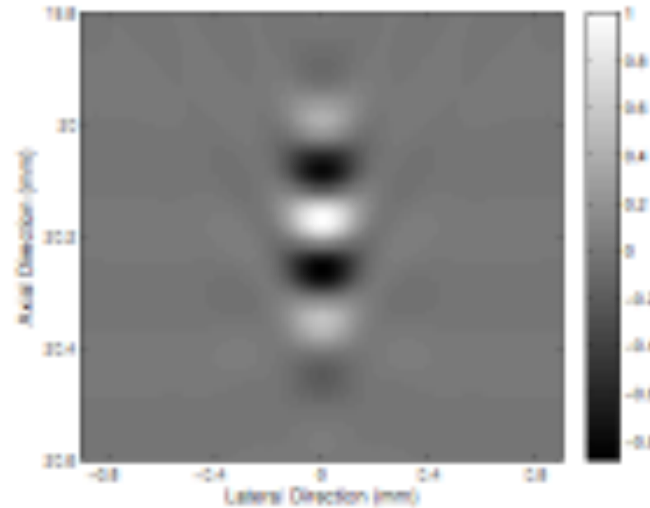

(b) Synthetic Aperture

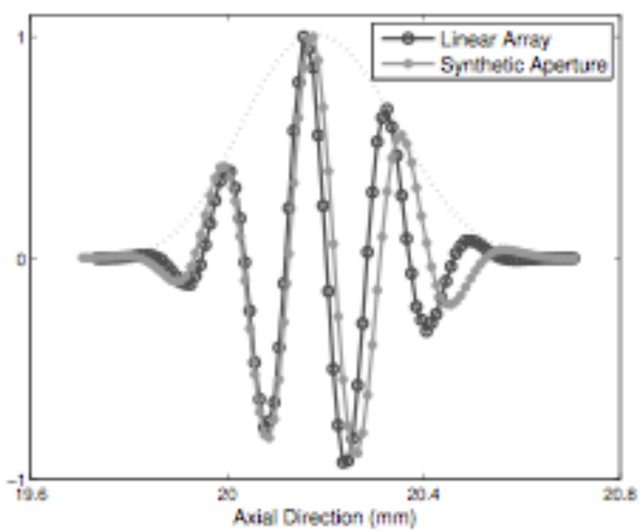

(a) Axial Profiles

Differences in PSF

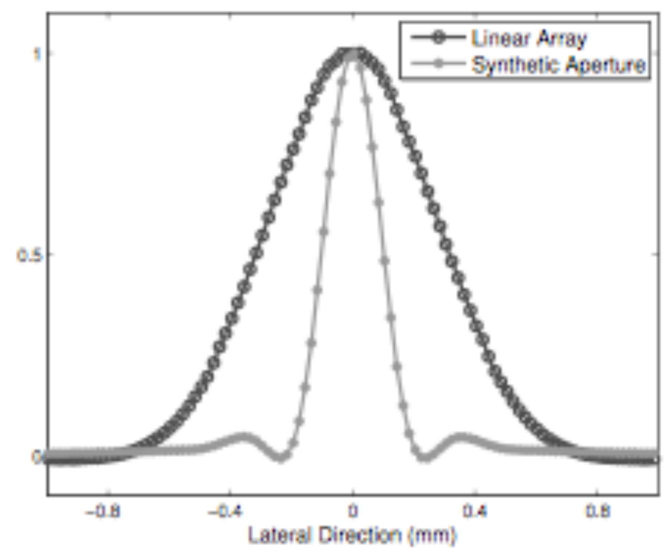

(b) Lateral Profiles

Axial displacements

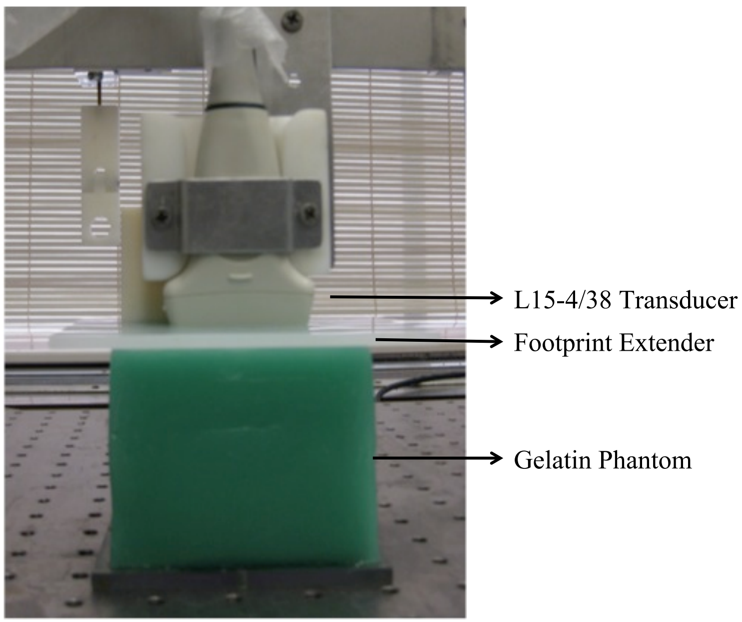

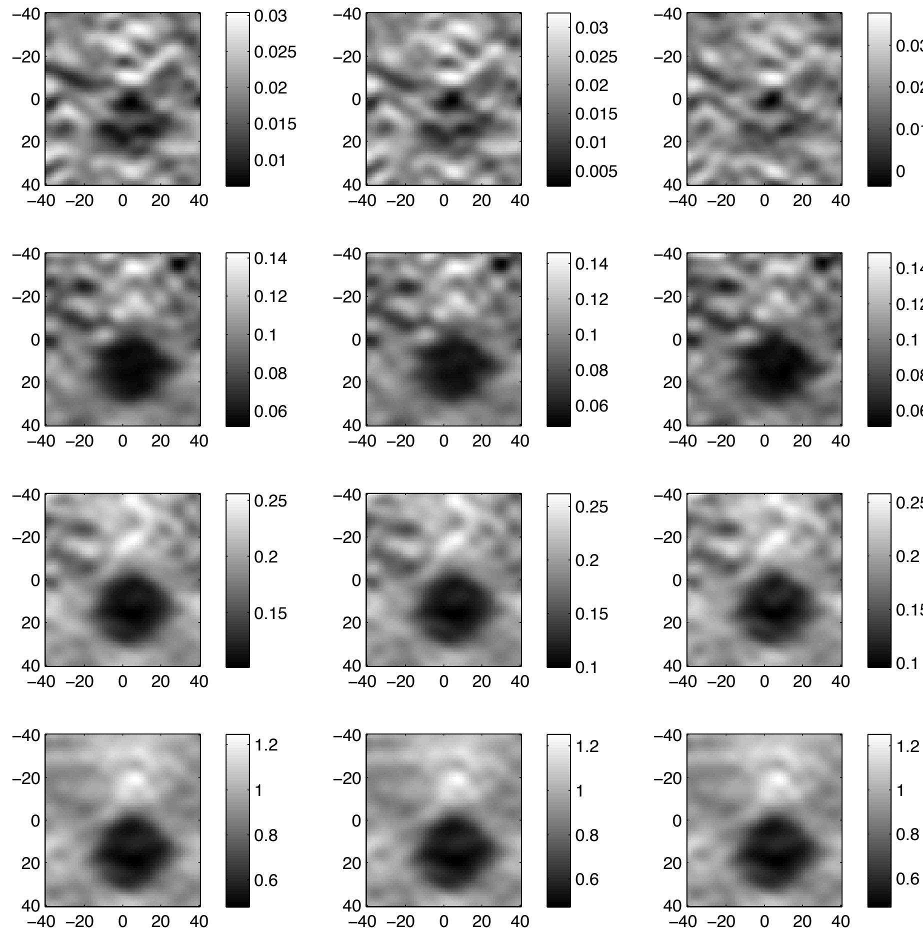

Compression = 0.1, 0.5, 1%

Line 6.4 , 12.8, 26, 51.2 lines/mm

Korokonda and Doyley 2011

Lateral displacements

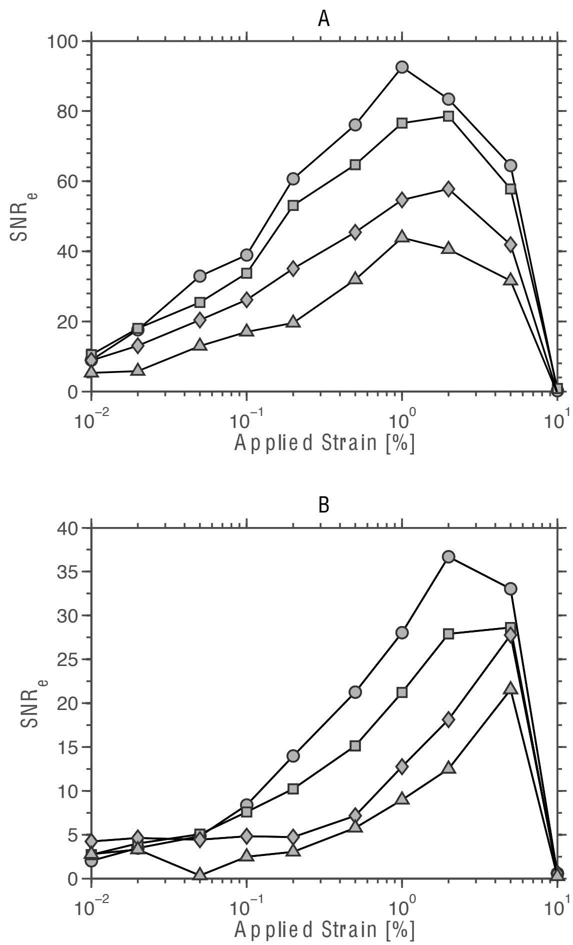

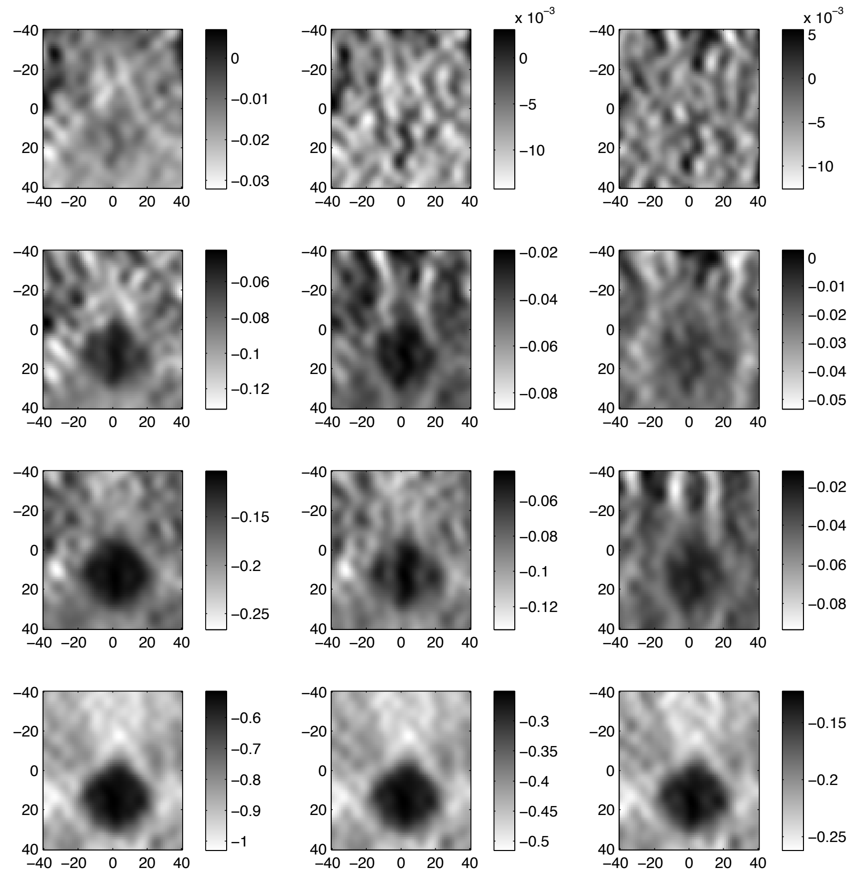

Sparse synthetic array

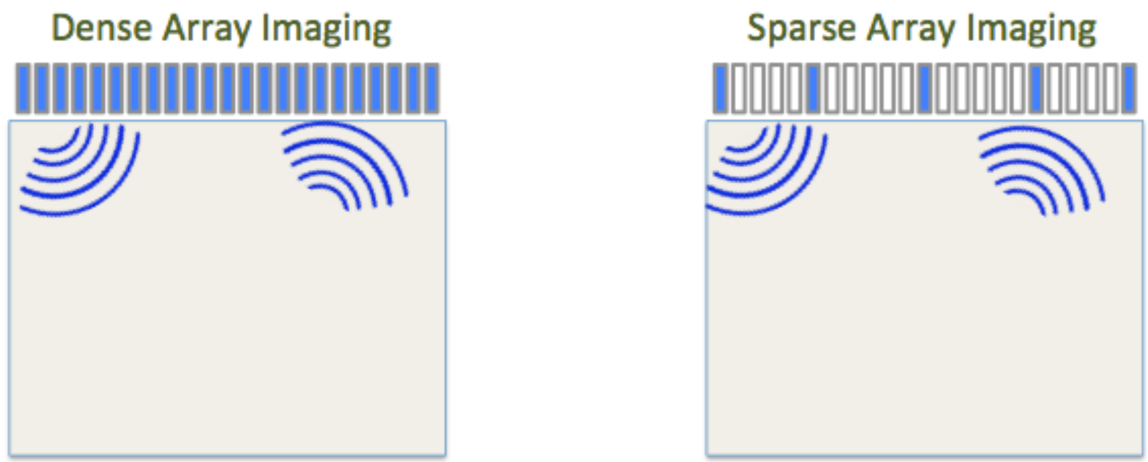

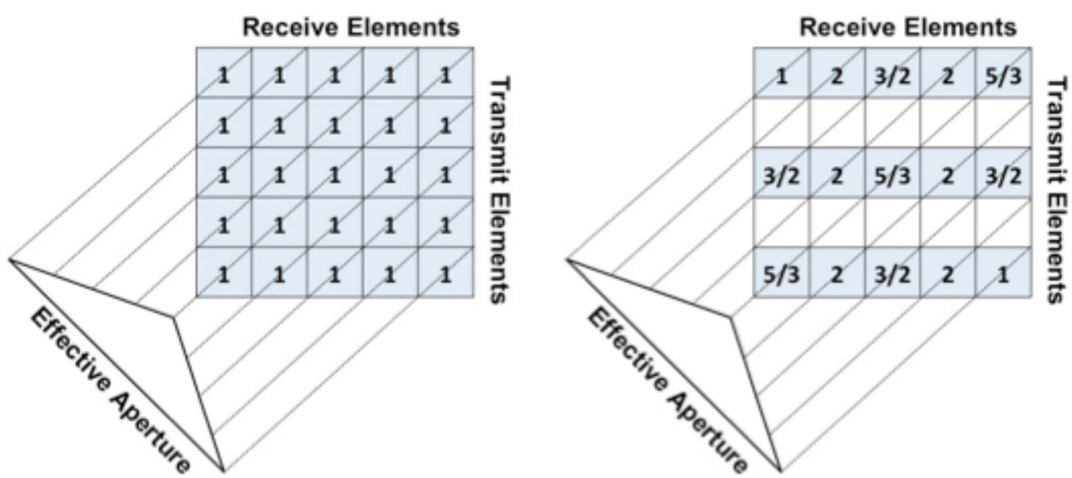

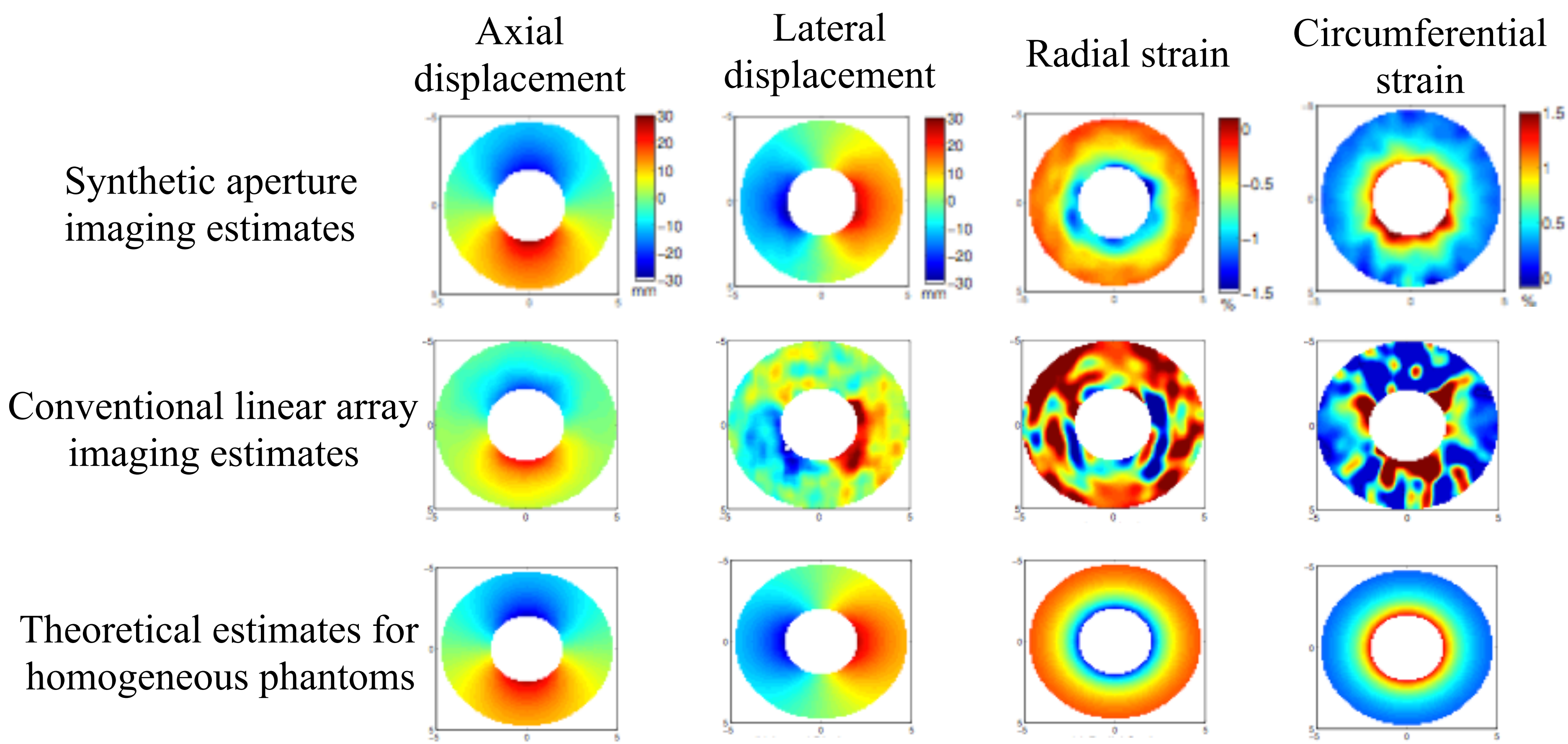

Korokonda and Doyley 2012

Strain SNR vs. active elements

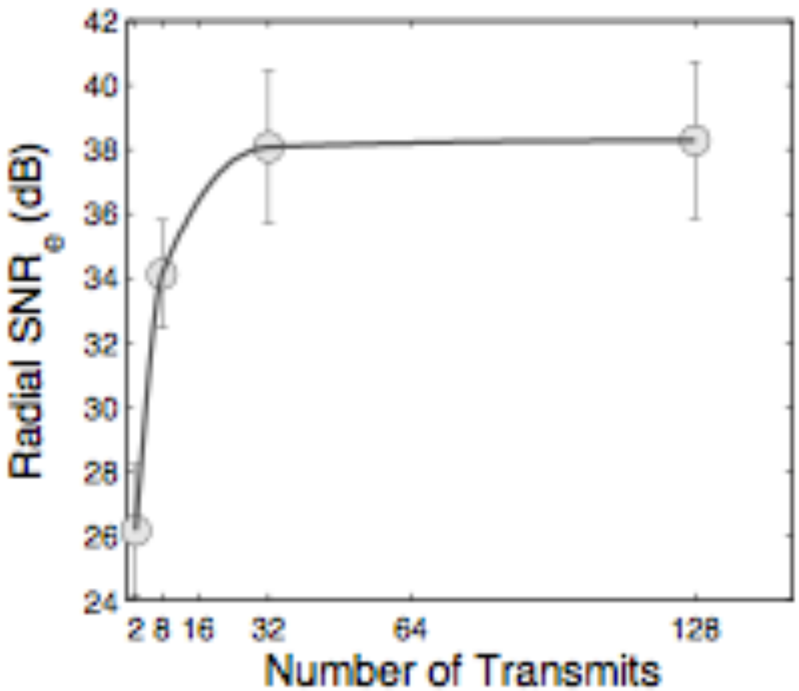

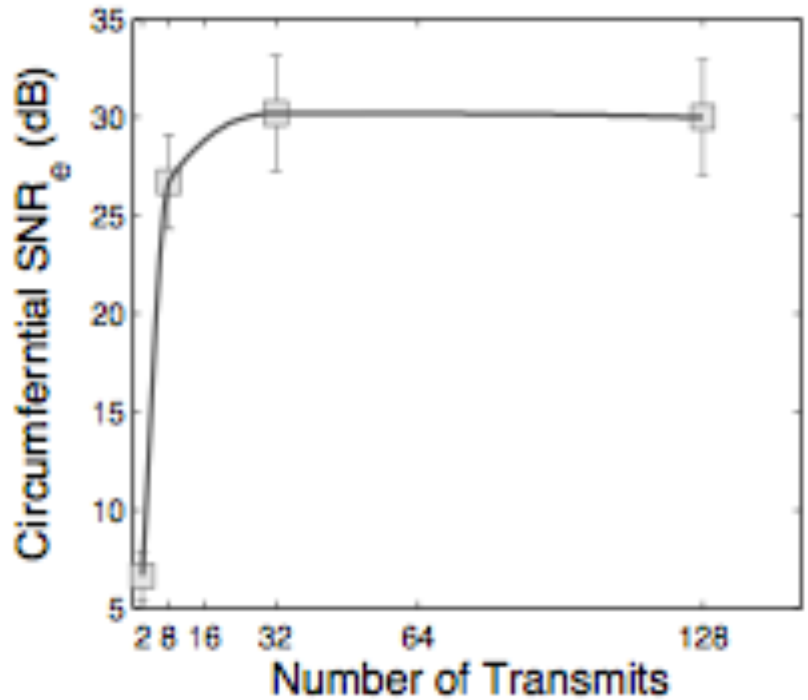

Ultrafast imaging techniques

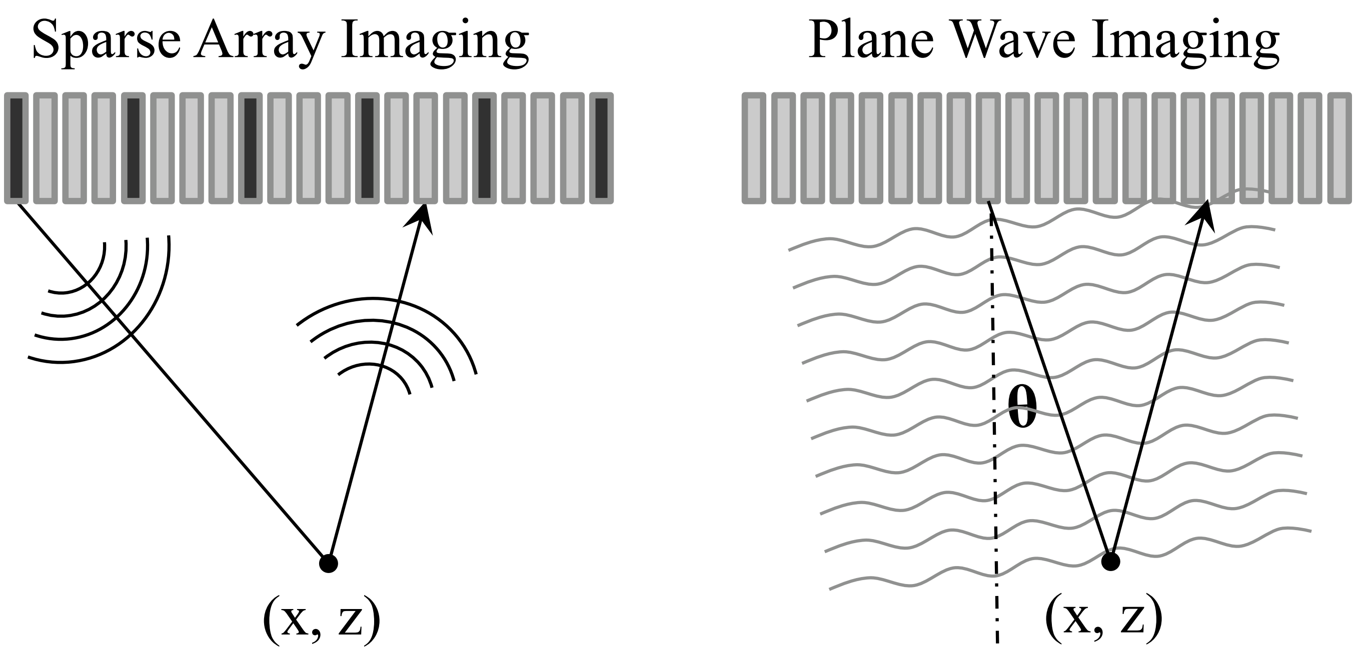

Korokunda *et al.* 2013

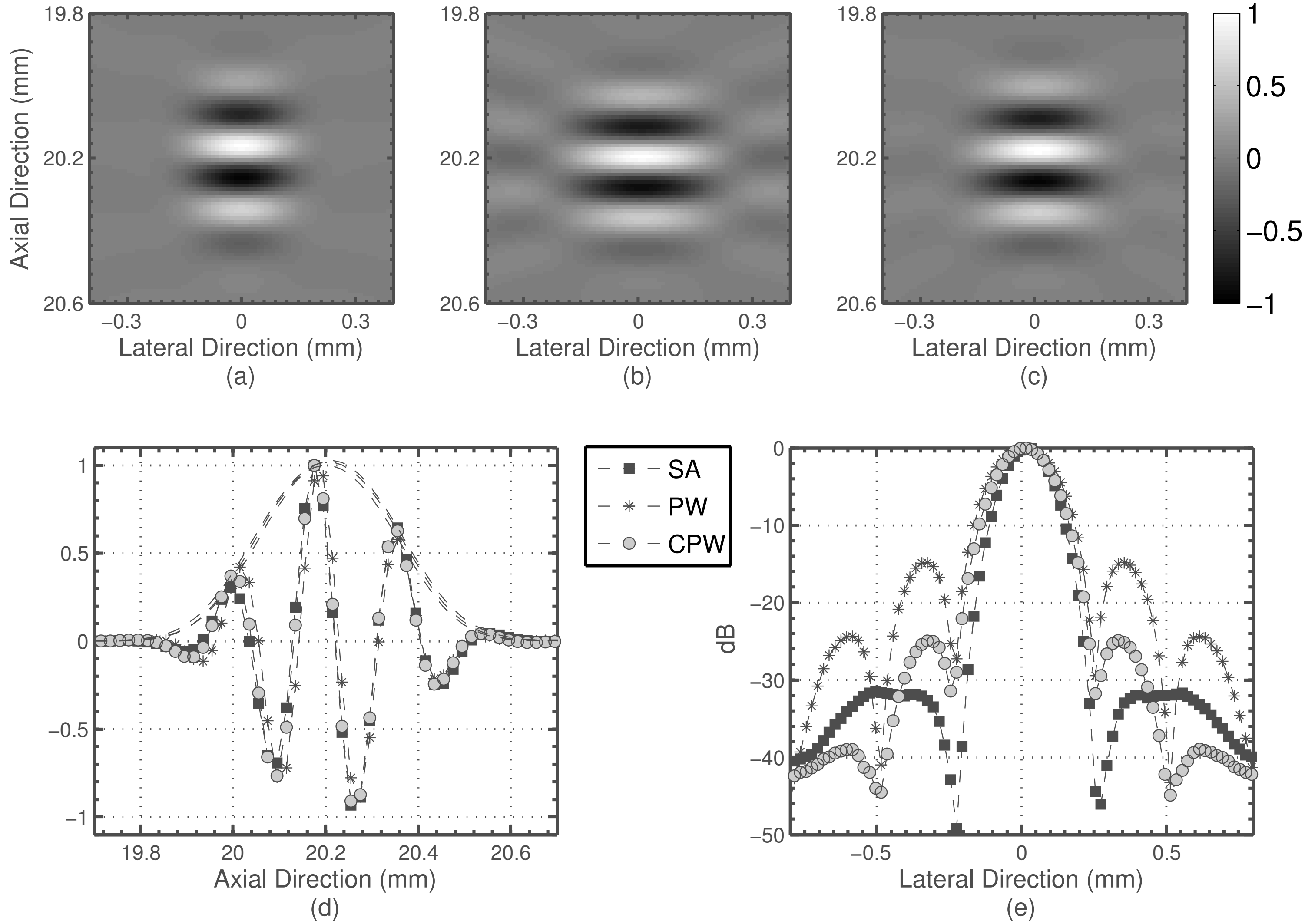

Axial Direction (mm)
19.8
20.2
20.6
-0.3
0
0.3
Lateral Direction (mm)
(a)
(b)
(c)
1
0.5
0
-0.5
-1
SA
PW
CPW
19.8
20
20.2
20.4
20.6
Axial Direction (mm)
(d)
dB
0
-10
-20
-30
-40
-50
-0.5
0
0.5
Lateral Direction (mm)
(e)

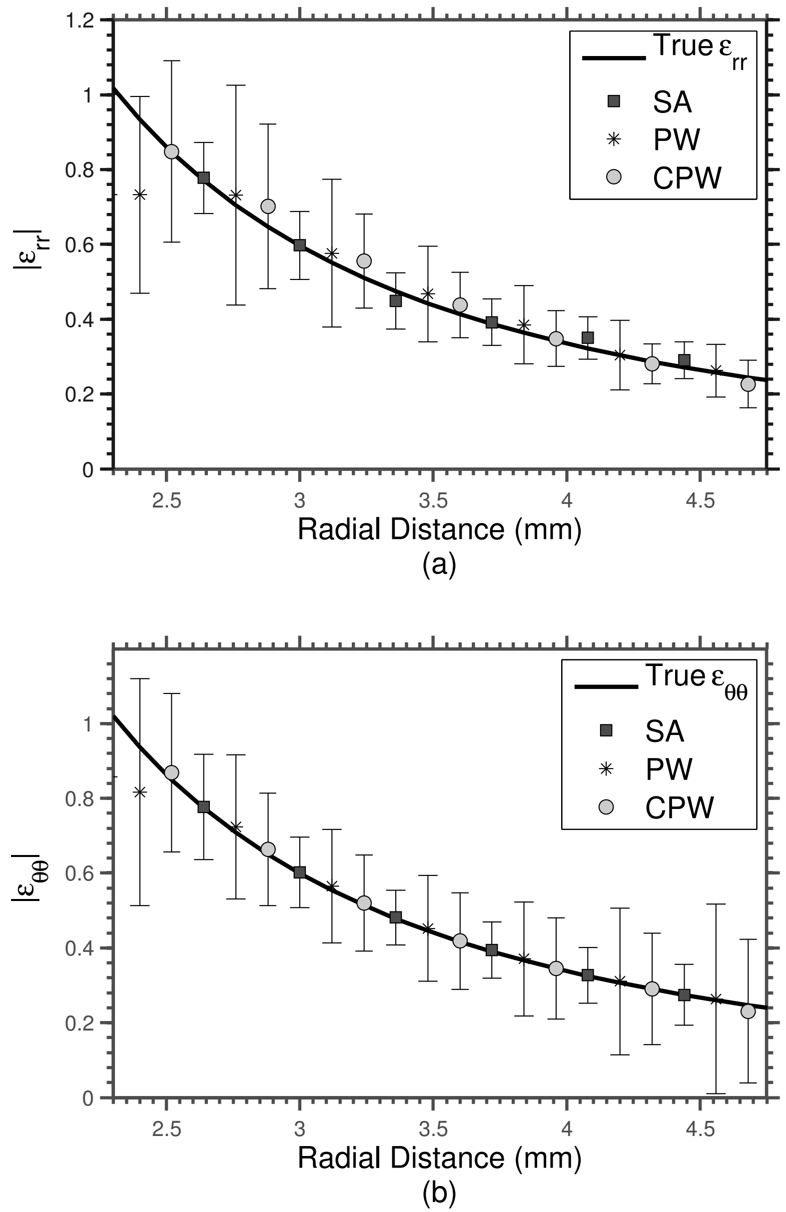

Computer simulations

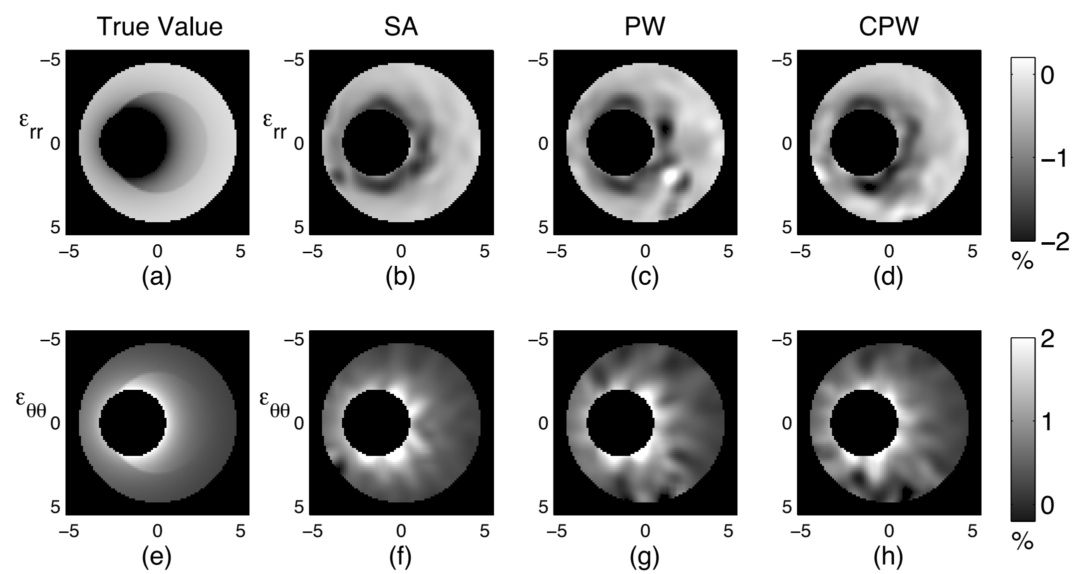

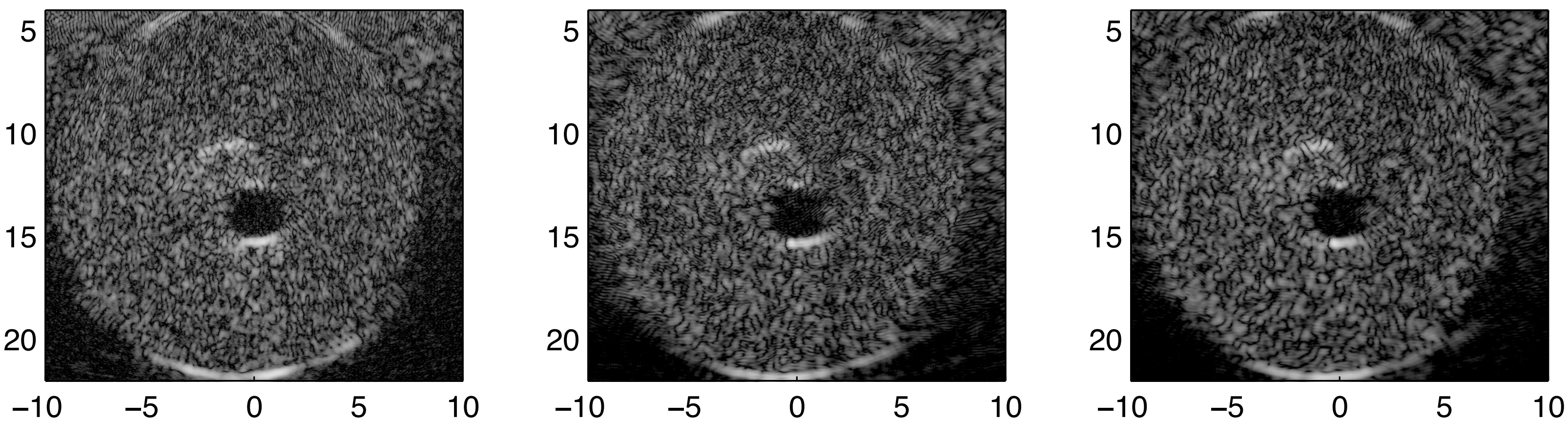

(a) (b) (c)

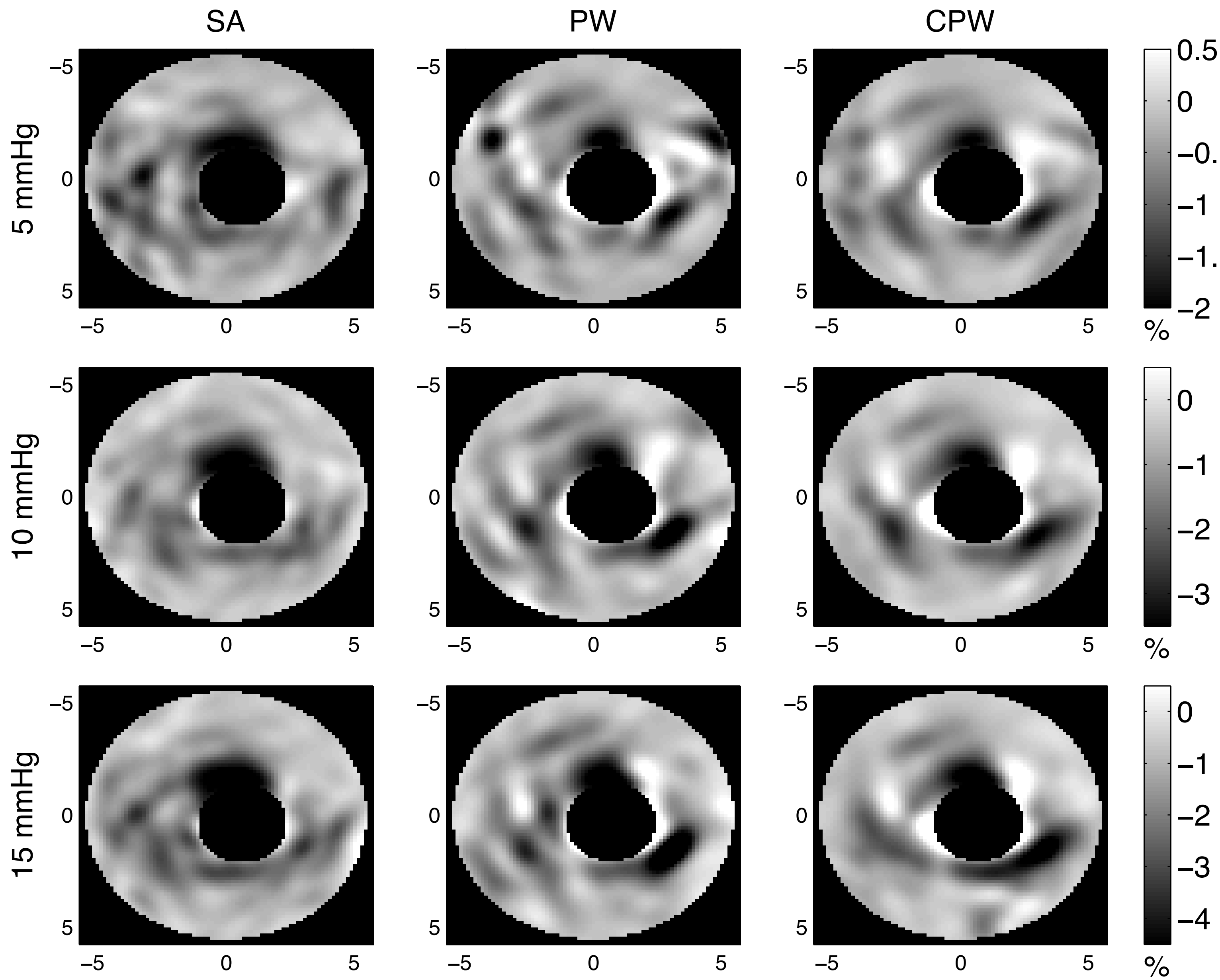
SA
PW
CPW
5 mmHg
10 mmHg
15 mmHg
−5
0
5
0.5
0
−0.
−1
−1.
−2
%
0
−1
−2
−3
%
0
−1
−2
−3
−4
%

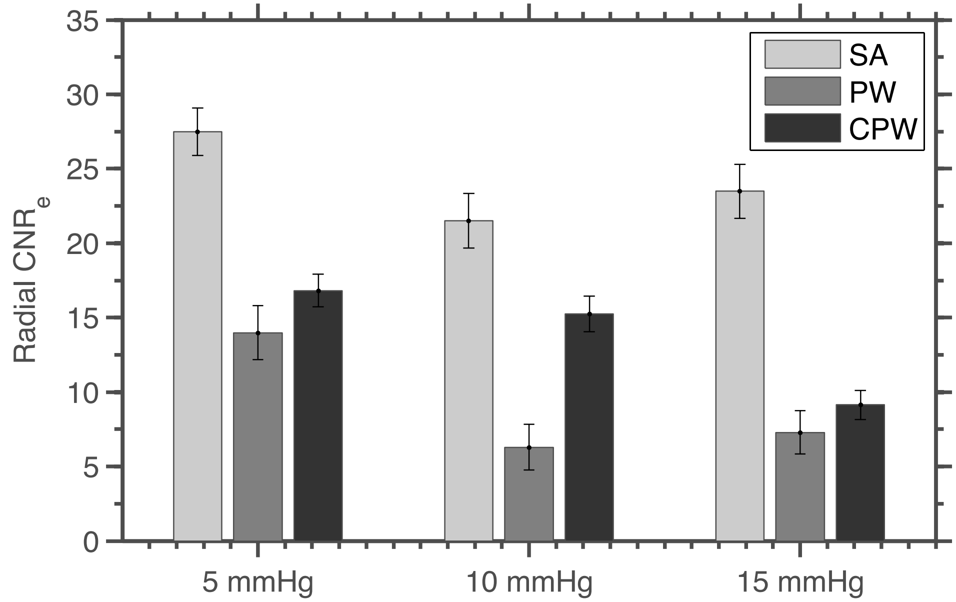

Radial CNR_e
35
30
25
20
15
10
5
0
5 mmHg
10 mmHg
15 mmHg
SA
PW
CPW

(a)

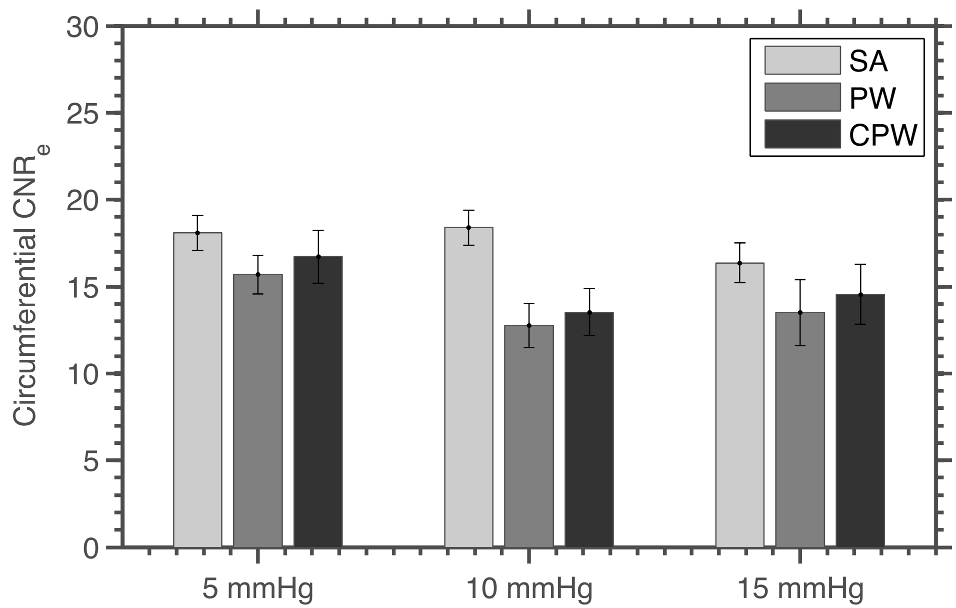

Circumferential CNR_e
30
25
20
15
10
5
0
5 mmHg
10 mmHg
15 mmHg
SA
PW
CPW

(b)

Healthy Volunteer

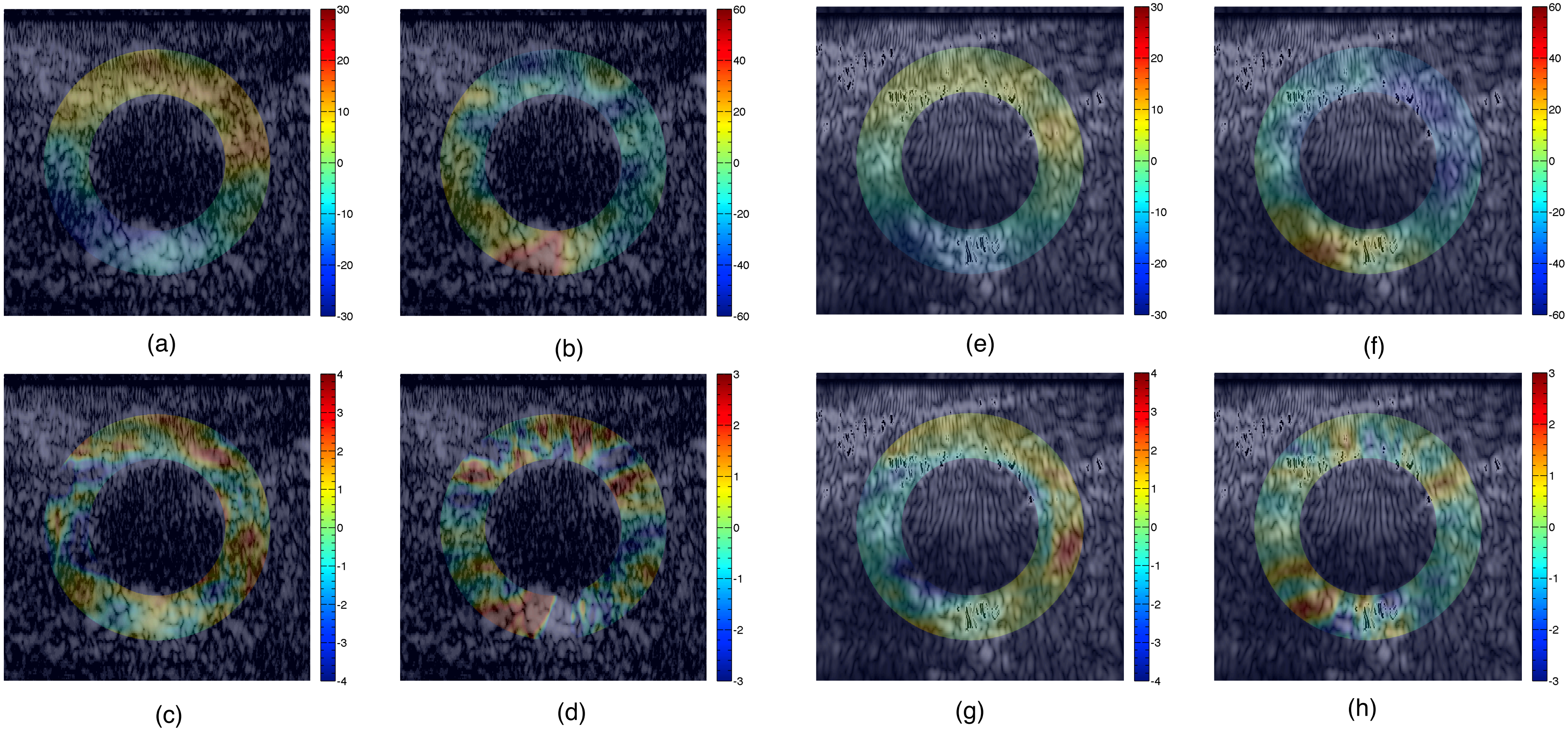

SAR Elastograms

Compounded Plane-Wave Elastograms

Virtual source sparse synthetic array

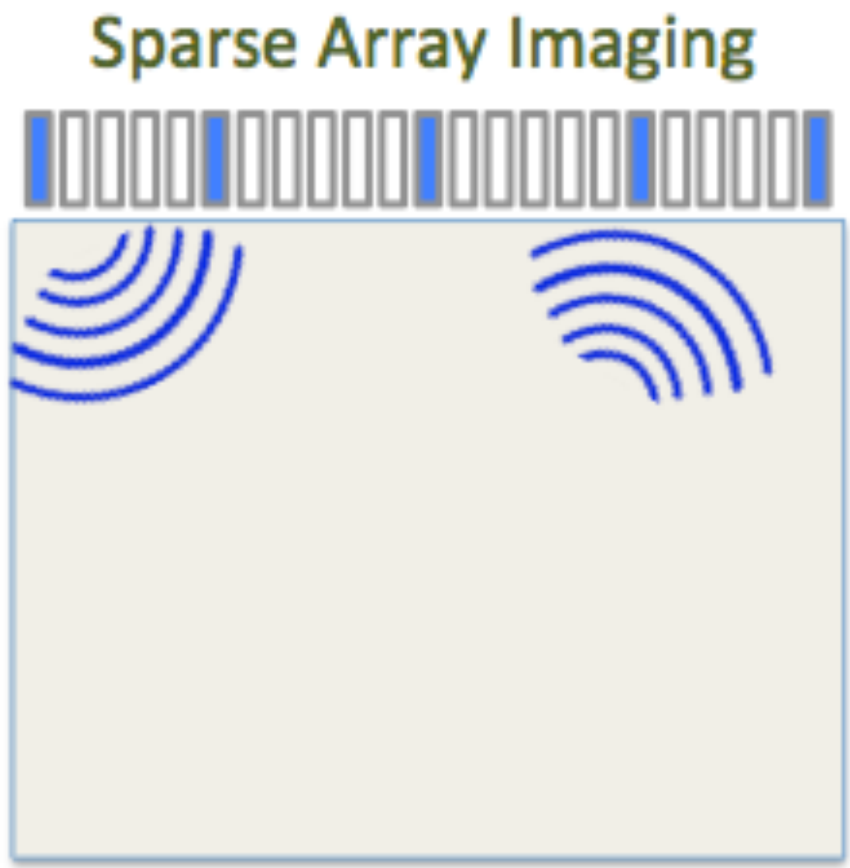

vSAVE (Virtual sources)

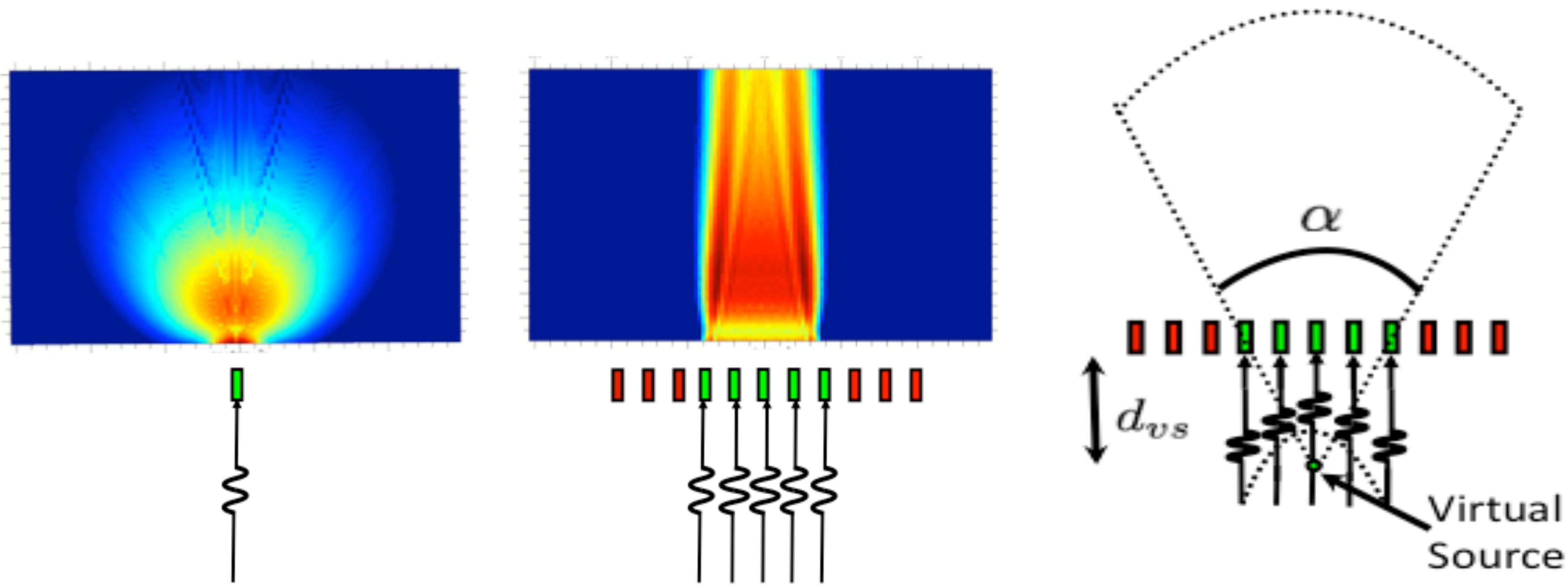

Goal: More transmit power with lower side-lobes

$$\alpha = 2\arctan\left(\frac{\text{Nel} \times \text{pitch}}{2d_{vs}}\right)$$

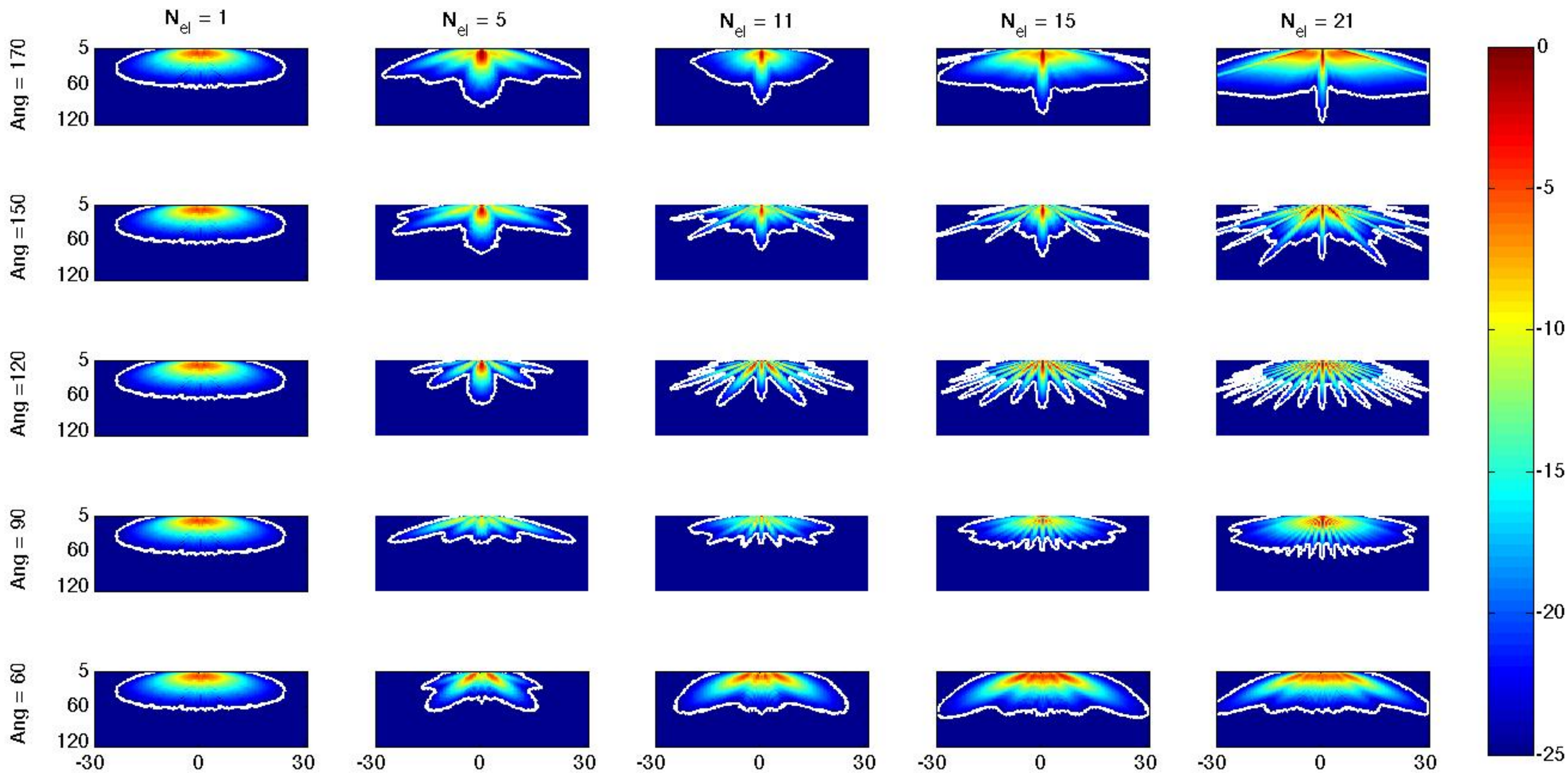

Radial Strain

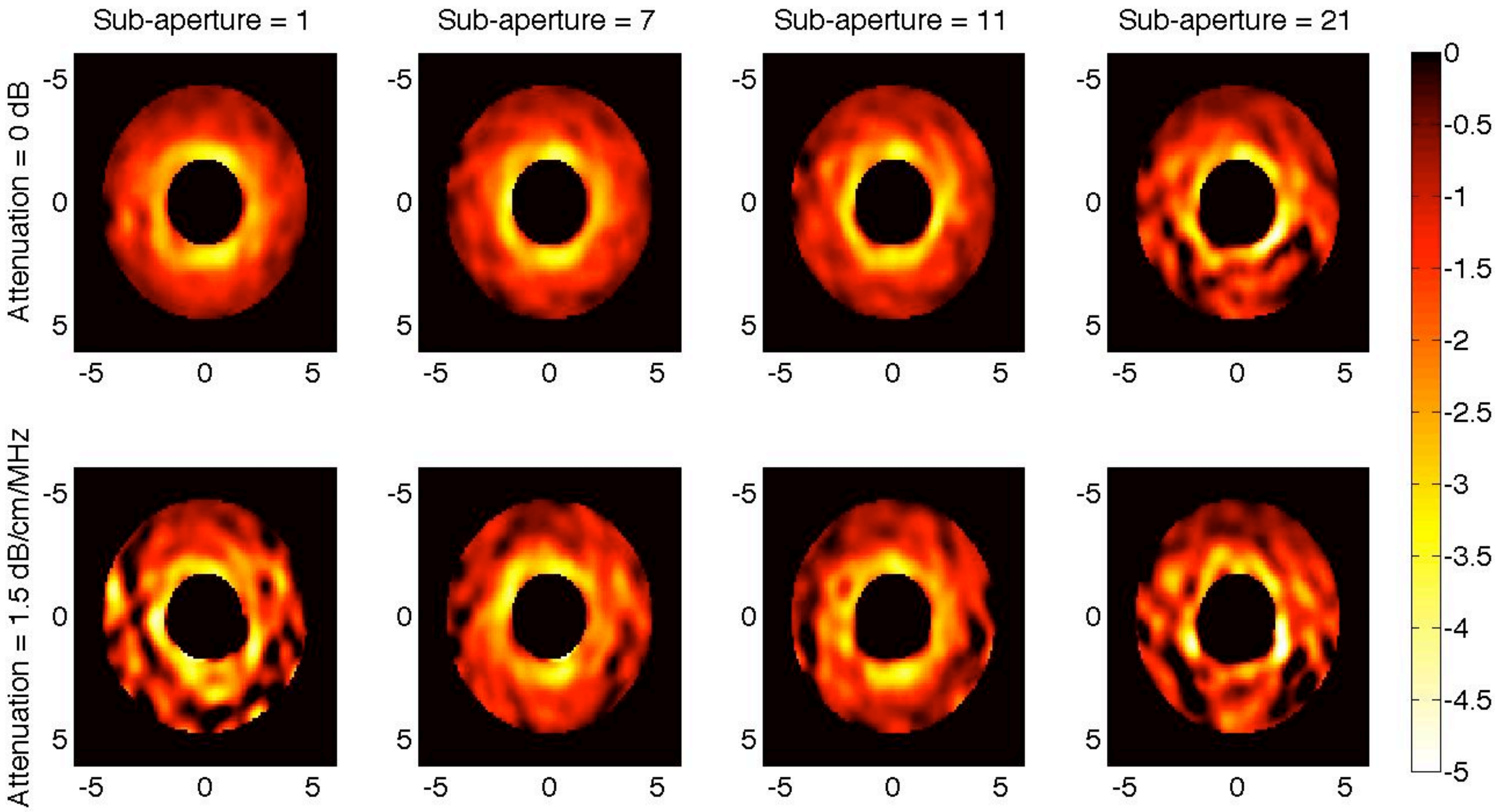

MV beam-forming (PW)

- Data dependent beam-forming
- Minimizing the variance in signals:

$$\min(w^H R\, w)$$

- Unity gain in desired directions:

$$w^H a = 1$$

- Since delays are introduces before summation:

$$a = \begin{bmatrix} 1 \\ 1 \\ 1 \\ \vdots \\ 1 \end{bmatrix}$$

- Dynamic weights:

$$z(t) = \sum_{m=0}^{M-1} w_m y_m (t - \Delta_m)$$

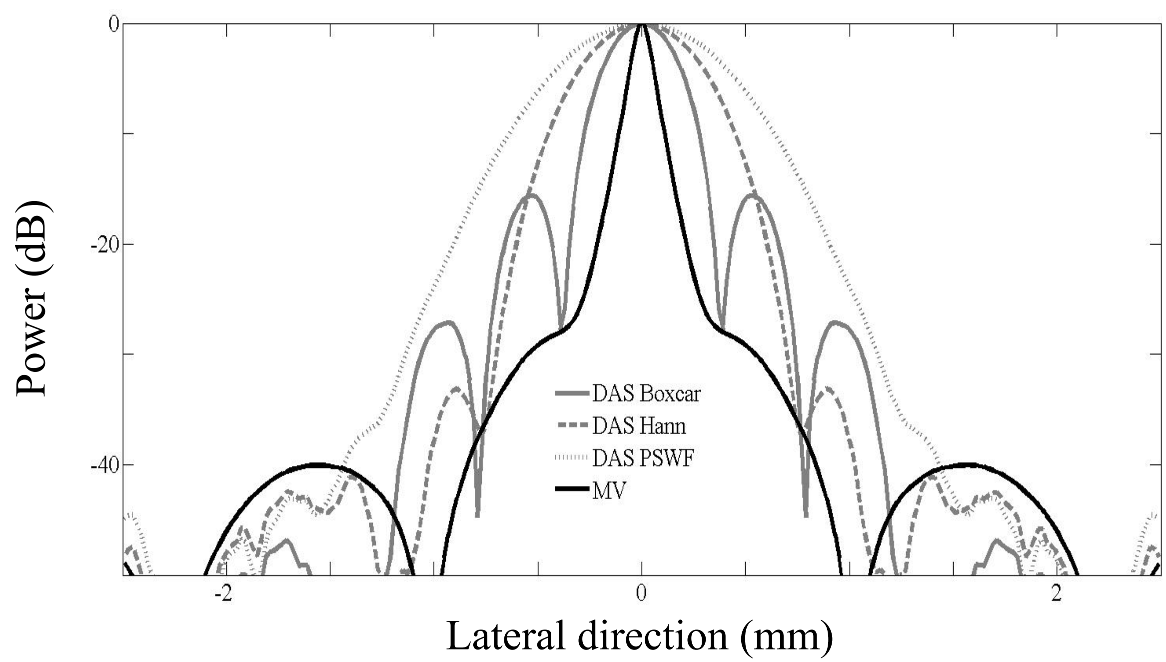

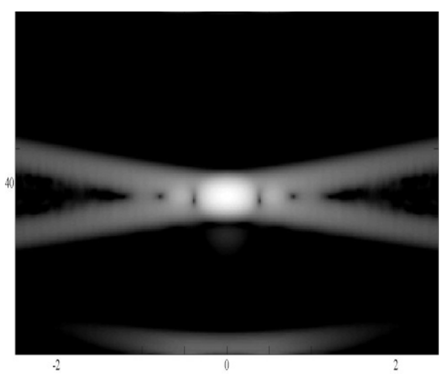
DAS Boxcar

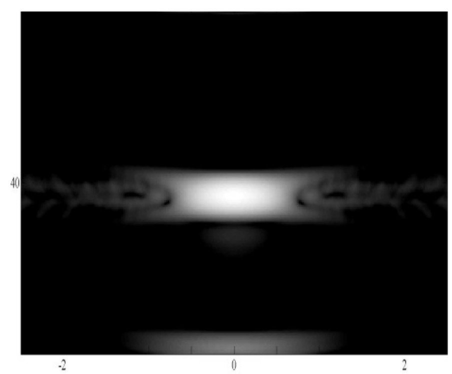
DAS Hann

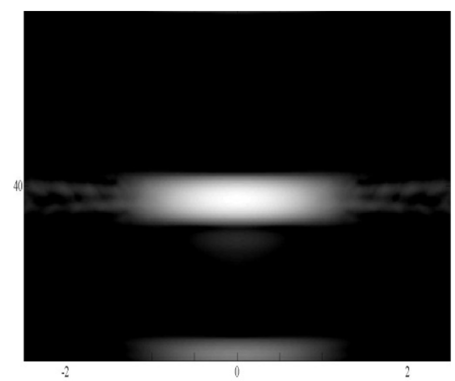
DAS PSWF

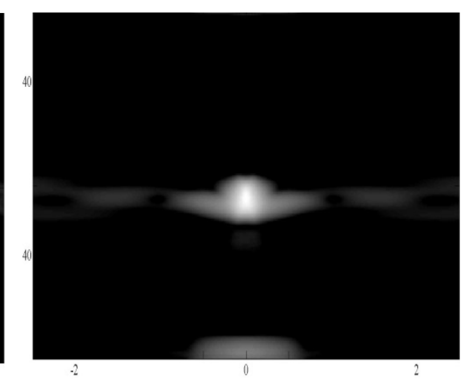
MV

Computer simulations

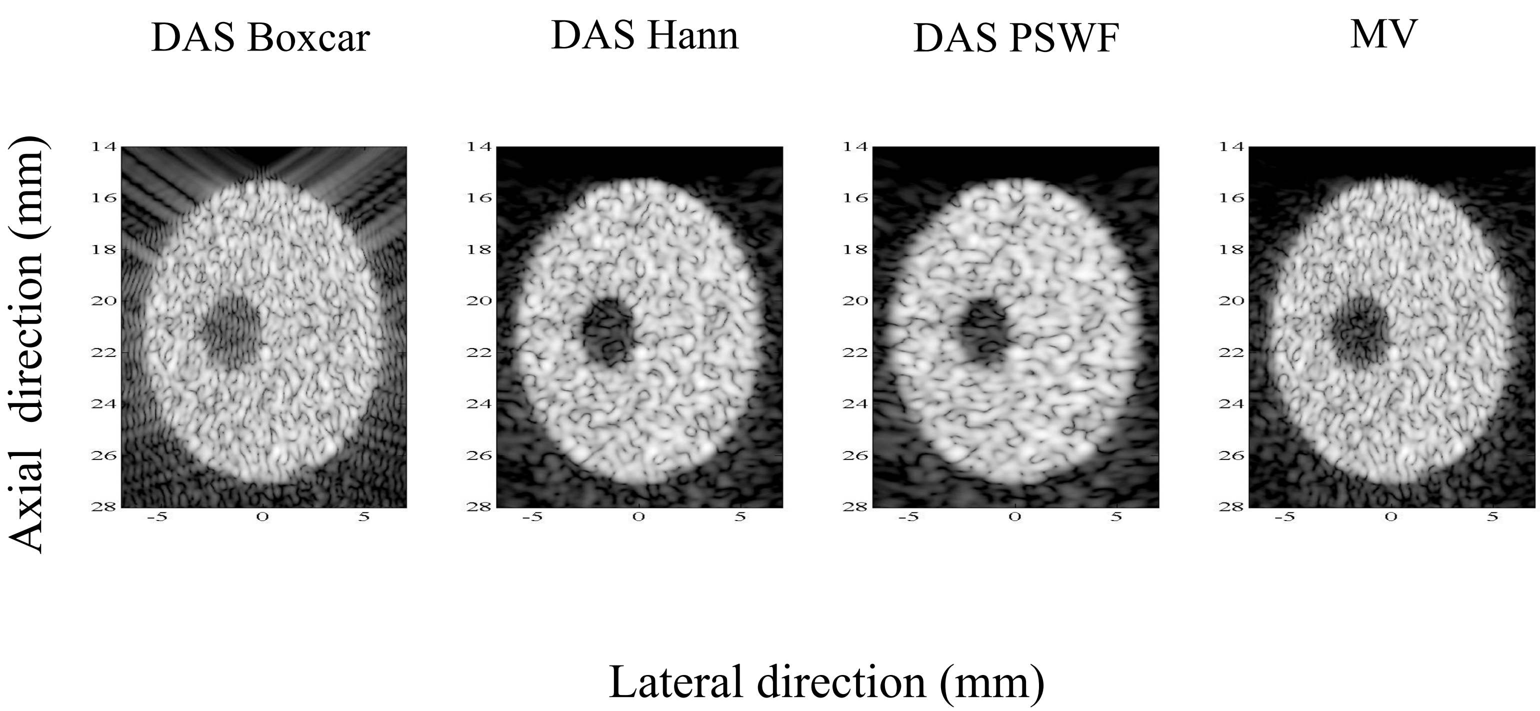

Simulation Results

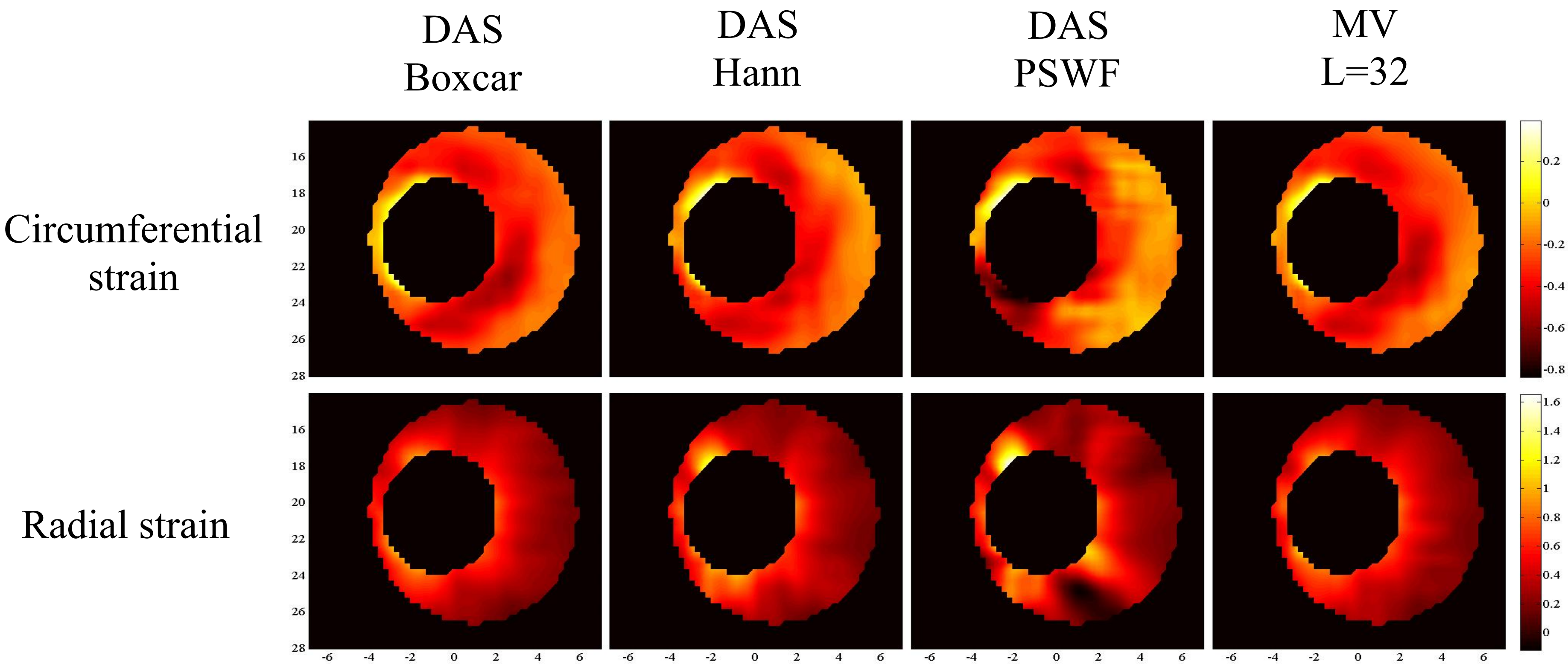

Phantom results (Strain maps)

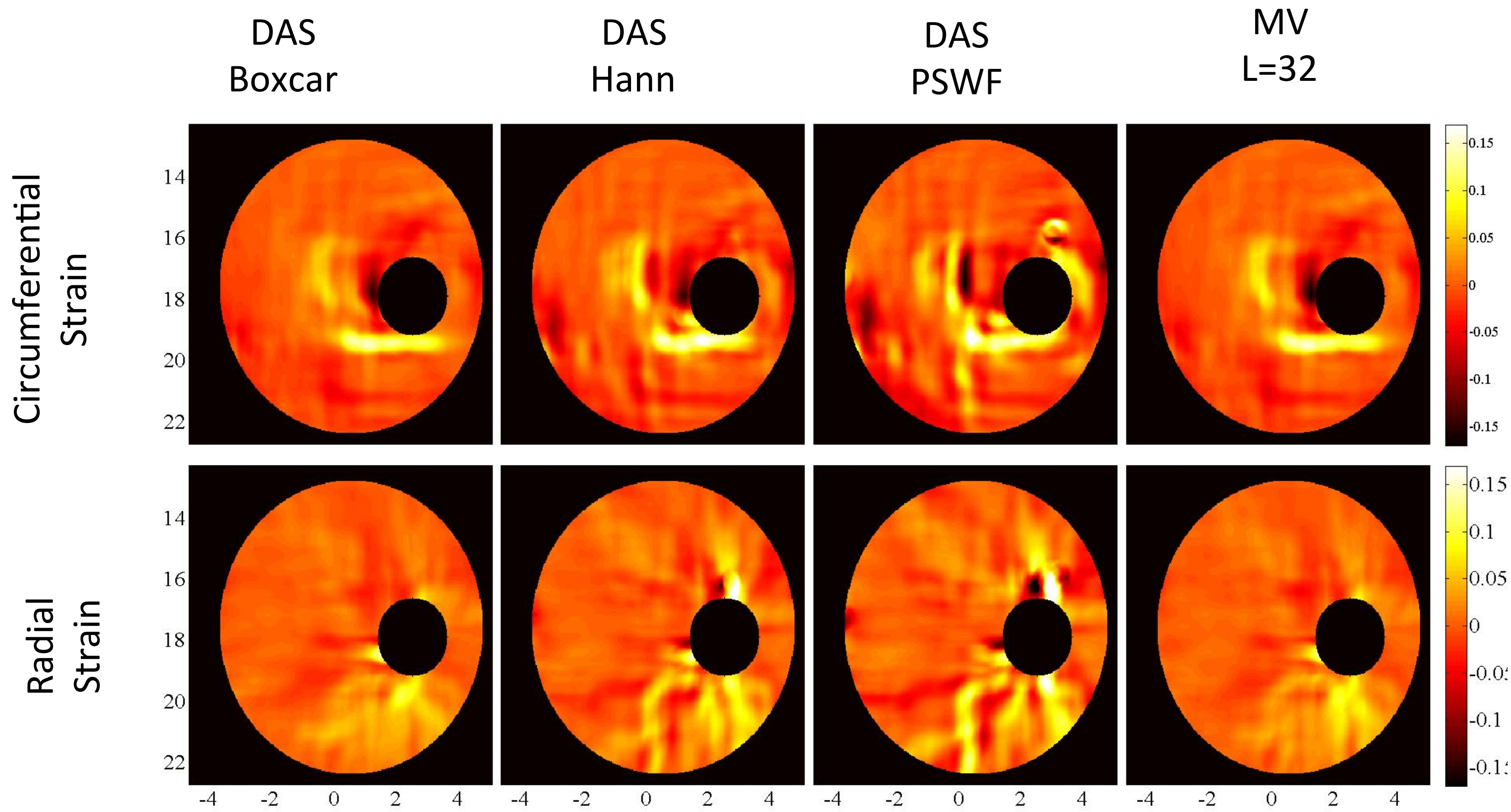

Members of
Parametric Imaging Research Laboratory